The $Ca_v\beta_{1a}$ subunit regulates gene expression and suppresses myogenin in muscle progenitor cells

Jackson Taylor,[1,2] Andrea Pereyra,[1,3] Tan Zhang,[1] Maria Laura Messi,[1] Zhong-Min Wang,[1] Claudia Hereñú,[3] Pei-Fen Kuan,[4] and Osvaldo Delbono[1,2]

[1]Department of Internal Medicine-Gerontology, [2]Neuroscience Program, Wake Forest School of Medicine, Winston-Salem, NC 27157
[3]Biochemistry Research Institute of La Plata (INIBIOLP)/National Scientific and Technical Research Council (CONICET), School of Medicine, National University of La Plata, 1900 La Plata, BA, Argentina
[4]Department of Applied Mathematics and Statistics, Stony Brook University, Stony Brook, NY 11794

Voltage-gated calcium channel (Ca_v) β subunits are auxiliary subunits to Ca_vs. Recent reports show $Ca_v\beta$ subunits may enter the nucleus and suggest a role in transcriptional regulation, but the physiological relevance of this localization remains unclear. We sought to define the nuclear function of $Ca_v\beta$ in muscle progenitor cells (MPCs). We found that $Ca_v\beta_{1a}$ is expressed in proliferating MPCs, before expression of the calcium conducting subunit $Ca_v1.1$, and enters the nucleus. Loss of $Ca_v\beta_{1a}$ expression impaired MPC expansion in vitro and in vivo and caused widespread changes in global gene expression, including up-regulation of myogenin. Additionally, we found that $Ca_v\beta_{1a}$ localizes to the promoter region of a number of genes, preferentially at noncanonical (NC) E-box sites. $Ca_v\beta_{1a}$ binds to a region of the Myog promoter containing an NC E-box, suggesting a mechanism for inhibition of myogenin gene expression. This work indicates that $Ca_v\beta_{1a}$ acts as a Ca_v-independent regulator of gene expression in MPCs, and is required for their normal expansion during myogenic development.

Introduction

The voltage-gated calcium channel (Ca_v) β subunit ($Ca_v\beta$) was initially purified from rabbit skeletal muscle as part of the dihydropyridine receptor (now termed $Ca_v1.1$) complex (Curtis and Catterall, 1984). A total of four $Ca_v\beta$ genes have been cloned (*Cacnb*1–4), each with multiple splice variants (Buraei and Yang, 2010). Ca_vs contain an ER retention signal that is masked by $Ca_v\beta$ binding, allowing both proteins to traffic to the plasma membrane (Bichet et al., 2000). $Ca_v\beta$ interaction with Ca_vs also serves to modulate gating properties of the channel (Lacerda et al., 1991; Varadi et al., 1991). $Ca_v\beta$ subunits contain two protein interaction domains: Src homology 3 (SH3) and guanylate kinase (GK), which act both together and individually to regulate channel function (Takahashi et al., 2004, 2005; Miranda-Laferte et al., 2011).

$Ca_v\beta_{1a}$ is the dominant β subunit isoform/splice variant in skeletal muscle, where it associates with $Ca_v1.1$ in transverse tubules and plays a critical role in excitation–contraction (EC) coupling, the process of converting an electrical stimulus to mechanical response. $Ca_v\beta_{1a}$ is necessary for proper calcium channel expression in the transverse tubules (Gregg et al., 1996), and also functions to organize $Ca_v1.1$ into defined groups of four (tetrads), which pair to a single ryanodine receptor (RyR; Schredelseker et al., 2005, 2009). This strict geometrical organization and 4:1 stoichiometry is necessary for proper EC coupling. The β1-null mouse (Gregg et al., 1996) and the relaxed (redts25) zebrafish (Zhou et al., 2006) both show paralysis due to total lack of EC coupling, underscoring the importance of $Ca_v\beta_{1a}$ in EC coupling. The β1-null mouse (hereafter called *Cacnb1*$^{-/-}$) also shows severely reduced skeletal muscle mass at birth, attributed to a lack of activity during development.

In the last decade, over a dozen additional, noncalcium channel binding partners have been described in the literature for multiple $Ca_v\beta$ subunit isoforms (Béguin et al., 2001; Hohaus et al., 2002; Hibino et al., 2003; Grueter et al., 2006; Gonzalez-Gutierrez et al., 2007; Hidalgo and Neely, 2007; Kiyonaka et al., 2007;

A. Pereyra and T. Zhang contributed equally to this paper.

Correspondence to Osvaldo Delbono: odelbono@wakehealth.edu

Abbreviations used in this paper: Ca_v, voltage-gated calcium channel; ChIP, chromatin immunoprecipitation; DM, differentiation medium; EC, excitation–contraction; EMSA, electrophoretic mobility shift assay; GK, guanylate kinase; GM, growth medium; H&E, hematoxylin & eosin; LMB, leptomycin-B; MPC, muscle progenitor cell; NC, noncanonical; NLS, nuclear localization sequence; RAd, recombinant adenoviral; SH3, Src homology 3; TSS, transcription start site.

The Rockefeller University Press $30.00
J. Cell Biol. Vol. 205 No. 6 829–846
www.jcb.org/cgi/doi/10.1083/jcb.201403021

Yu et al., 2008; Catalucci et al., 2009; Buraei and Yang, 2010; Zhang et al., 2010; Tadmouri et al., 2012). Several additional reports show the nuclear localization of all four $Ca_v\beta$ subunits, either alone (Colecraft et al., 2002; Subramanyam et al., 2009) or when cotransfected with members of the RGK family of proteins (Béguin et al., 2006; Leyris et al., 2009). Two studies have demonstrated transcriptional regulation in vitro by the neuronal $Ca_v\beta3$ (Zhang et al., 2010) and $Ca_v\beta4c$ subunits (Hibino et al., 2003), and a recent comprehensive work showed that $Ca_v\beta4$ inhibits tyrosine hydroxylase expression in brain tissue (Tadmouri et al., 2012).

Although the role of $Ca_v\beta_{1a}$ in mature skeletal muscle is well understood, its role in muscle progenitor cells (MPCs), if any, is not known. MPCs are capable of rapid proliferation during development, or after activation in response to muscle damage in adults, after which they can differentiate and fuse together into mature myofibers. Unlike mature myofibers, MPCs are capable of DNA replication and cell division while maintaining a commitment to the skeletal muscle lineage. Regulation of cell fate by myogenic transcription factors such as Pax7, MyoD, and myogenin is well understood; however, questions still remain about how these factors themselves are regulated.

We sought to define the physiological role for $Ca_v\beta$ subunits in the nucleus, specifically in MPCs. Here we report a pathway by which $Ca_v\beta_{1a}$ regulates skeletal muscle mass during embryonic development by suppression of the *Myog* promoter.

Results

$Ca_v\beta_{1a}$ expression in muscle progenitor cells

Although $Ca_V\beta$ subunits have been studied in myotubes, specifically the muscle-specific splice variant $Ca_V\beta_{1a}$ (coded by the *Cacnb1* gene), little is known about their expression in MPCs (myoblasts). A microarray study suggested that while *Cacnb1* mRNA expression increases during differentiation, it still expresses in significant quantities in subconfluent, proliferating C2C12 myoblasts (Tomczak et al., 2004). Therefore, we sought to characterize *Cacnb1* expression at the mRNA and protein level in C2C12 and primary mouse myoblasts. RT-PCR with primers to the muscle-specific *Cacnb1* splice variant A (β_{1a}), which codes for the $Ca_V\beta_{1a}$ protein, detected $Ca_V\beta_{1a}$ mRNA in subconfluent myoblasts, which increased during myogenic differentiation (Fig. 1 A). We next characterized $Ca_V\beta_{1a}$ subunit protein expression in C2C12 and primary myoblasts, using two different $Ca_V\beta_{1a}$ antibodies. A protein band close to the expected molecular weight of $Ca_V\beta_{1a}$ (55 kD) appeared specifically in both C2C12 and primary myoblasts, using both antibodies, compared with isotype IgG controls (Fig. 1 B, $Ca_V\beta_{1a}$ antibody clone H-50 was used for the remainder of experiments). $Ca_V\beta_{1a}$-specific shRNA-mediated knockdown of this protein band further confirmed its identity as $Ca_V\beta_{1a}$ (Fig. 1 C). Additionally, although the antibody we used did label brain and cardiac protein bands (presumably other $Ca_V\beta$ isoforms), these had different molecular weights (Fig. 1 C). To examine $Ca_V\beta_{1a}$ expression and localization during myogenesis, we analyzed cytosolic and membrane lysates collected from proliferating (subconfluent in growth medium [GM]) and differentiating C2C12 cells (24–96 h in differentiation medium [DM]) by Western blot (Fig. 1 D). In proliferating myoblasts, $Ca_V\beta_{1a}$ appeared in the cytosolic but not plasma membrane fractions, whereas the $Ca_V1.1$ protein was absent, as expected (Bidaud et al., 2006). The absence of $Ca_V\beta_{1a}$ in the membrane fraction of myoblasts suggests it does not interact with any channels, $Ca_V1.1$ or otherwise, indicating a nonchannel function. Cytosolic $Ca_V\beta_{1a}$ protein expression increased mildly during differentiation, but showed a large increase in the membrane fraction after 48 h in DM, concomitantly with the appearance of $Ca_V1.1$, reaffirming the classical role of $Ca_V\beta_{1a}$ as a $Ca_V1.1$ binding partner in mature skeletal muscle. Immunostaining of $Ca_V\beta_{1a}$ showed a very faint nuclear and perinuclear signal in proliferating and early-fusing myoblasts. However, in fully differentiated myotubes a strong punctate signal was observed, presumably corresponding to $Ca_V\beta_{1a}$ associated with $Ca_V1.1$ at the plasma membrane (Fig. 1 E). These results support the idea that myoblasts do not express Ca_Vs, yet still express $Ca_V\beta_{1a}$. Thus, in MPCs, $Ca_V\beta_{1a}$ exists in a spatially and temporally separate pool from its constituent Ca_V, raising the likelihood of Ca_V-independent functions.

Nuclear $Ca_v\beta_{1a}$

As other $Ca_V\beta$ subunits have been observed in the nucleus of various cell types, we hypothesized $Ca_V\beta_{1a}$ may localize there in MPCs as well. Because our antibodies did not appear sensitive enough for clear immunofluorescent detection in C2C12 myoblasts, we constructed a recombinant adenoviral (RAd) vector to overexpress a $Ca_v\beta_{1a}$-YFP plasmid (Leuranguer et al., 2006) in these cells. $Ca_v\beta_{1a}$-YFP shows a predominantly cytoplasmic localization (Fig. 2 A), although some cells also exhibited substantial fluorescence in the nucleus. However, after 3 h of treatment with the CRM1 nuclear export channel blocker leptomycin-B (LMB), all cells exhibited $Ca_v\beta_{1a}$-YFP fluorescence predominantly in the nucleus (Fig. 2 B). $Ca_v\beta_{1a}$ antibody staining of these treated cells overlapped with YFP fluorescence in the nucleus (unpublished data). To further confirm the translocation of $Ca_v\beta_{1a}$-YFP into the nucleus of C2C12 myoblasts, we obtained pure cytosolic and nuclear fractions from $Ca_v\beta_{1a}$-YFP–expressing cells, and analyzed $Ca_v\beta_{1a}$-YFP protein expression by Western blot (Fig. 2 C). $Ca_v\beta_{1a}$-YFP was clearly present in the nucleus, even without LMB treatment. In both untreated and LMB-treated cells, $Ca_v\beta_{1a}$-YFP could be immunoprecipitated from nuclear fractions with an YFP antibody, further indicating the specific localization of $Ca_v\beta_{1a}$-YFP (Fig. 2 C). It is important to note that the expected and observed size of $Ca_v\beta_{1a}$-YFP is nearly 80 kD (Fig. 2 C), far above the size limit for passive diffusion into the nucleus (<50 kD), suggesting that $Ca_v\beta_{1a}$-YFP is rapidly and actively transported into the nucleus of C2C12 myoblasts. Furthermore, when examined carefully, the $Ca_v\beta_{1a}$-YFP band in nuclear fractions appears to be of a slightly higher molecular weight than cytosolic $Ca_v\beta_{1a}$-YFP, indicating that a possible post-translational modification is required for, or induced by, nuclear translocation.

We next wanted to determine if endogenous $Ca_v\beta_{1a}$ protein enters the nucleus of myoblasts. Immunostaining for endogenous $Ca_v\beta_{1a}$ after LMB treatment in nontransfected cells did not detect any clear nuclear enrichment (unpublished data), likely

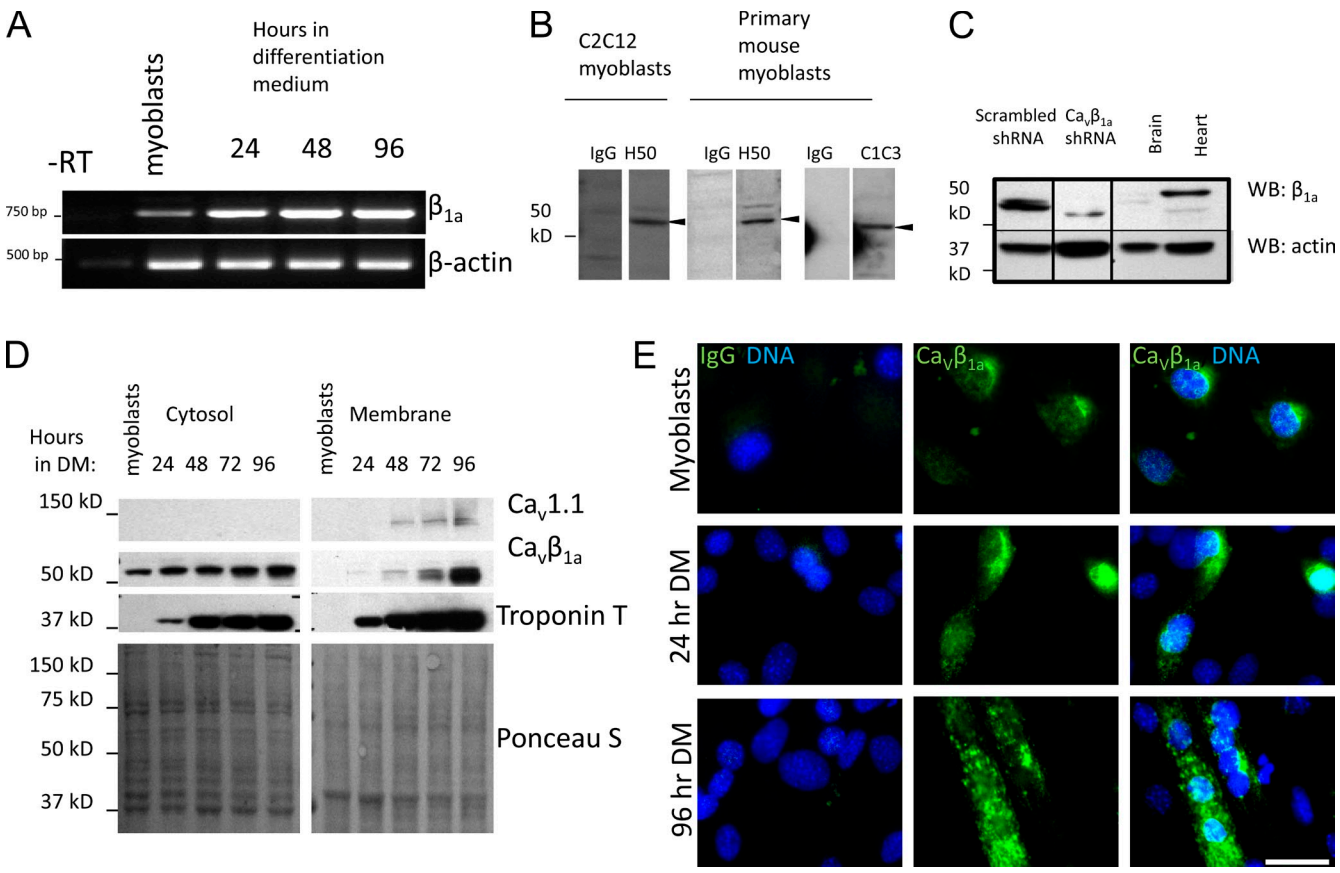

Figure 1. **$Ca_v\beta_{1a}$ expression in MPCs.** (A) mRNA expression of $Ca_v\beta_{1a}$ in primary MPCs cultured in GM (myoblasts) and after 24, 48, or 96 h in DM (−RT, nonreverse-transcribed control). (B) Expression of $Ca_v\beta_{1a}$ protein in C2C12 myoblasts and primary MPCs detected by Western blot using antibody clones H-50 and C1C3. A distinct band was detected (arrowheads) with a molecular weight of ∼55 kD. Each lane represents individual strip cut from same membrane. (C) Western blot for $Ca_v\beta_{1a}$ expression in C2C12 stably transfected with scrambled control or $Ca_v\beta_{1a}$-specific shRNA. Brain and heart protein lysates were also run as negative controls. (D and E) C2C12 myoblasts were grown to confluence in GM, then switched to DM for analysis at 24-h intervals. (D) Western blot for $Ca_v\beta_{1a}$ and $Ca_v1.1$ in cytosolic and membrane fractions. Troponin T is a marker of myogenic differentiation and Ponceau S stain shows equal loading. (E) Immunofluorescent staining for endogenous $Ca_v\beta_{1a}$ (green) and DNA (Hoechst stain, blue). Some nuclei are out of focus with visible $Ca_v\beta_{1a}$ staining. Bar, 100 µm.

due to a lack of sensitivity or epitope masking. To circumvent these issues, we performed a nuclear fractionation protocol and Western blot analysis, which is more sensitive and avoids epitope masking (Fig. 2 D). Compared with untreated cells, $Ca_v\beta_{1a}$ is enriched in the nuclear fraction of 6- and 12-h LMB-treated C2C12 myoblasts. As $Ca_v\beta_{1a}$ expression levels change in cytoplasmic and membrane fractions with myogenic differentiation, we also examined if $Ca_v\beta_{1a}$ nuclear expression changes during this process (Fig. 2 E). Interestingly, while cytoplasmic $Ca_v\beta_{1a}$ increases modestly with differentiation, nuclear $Ca_v\beta_{1a}$ appears to decline, further underscoring a possible MPC-specific role for $Ca_v\beta_{1a}$ in the nucleus. Close examination reveals that, like $Ca_v\beta_{1a}$-YFP, endogenous $Ca_v\beta_{1a}$ also seems to exist as a slightly higher molecular weight species (Fig. 2, D and E) within the nucleus, supporting the notion of a post-translational modification. In sum, these data strongly suggest that $Ca_v\beta_{1a}$ enters the nucleus of MPCs through some means of active transport.

$Ca_v\beta_{1a}$ possesses variable N- and C-terminal domains, as well as conserved SH3, HOOK, and GK domains. We wanted to determine which domain of $Ca_v\beta_{1a}$ endows its ability to enter the nucleus, and also whether this is a specific ability of $Ca_v\beta_{1a}$, or a mechanism conserved in all $Ca_v\beta$ subunits. All four $Ca_v\beta$ subunit isoforms have been reported to enter the nucleus (Buraei and Yang, 2010), and data suggests that this ability may lie within the SH3 domain (Colecraft et al., 2002; Hibino et al., 2003). However, $Ca_v\beta_{1a}$ also possesses a yeast nuclear localization sequence (NLS), KRKGRFKR (Hicks and Raikhel, 1995). This sequence, located in $Ca_v\beta_{1a}$'s N-terminal domain, is not highly conserved in other $Ca_v\beta$ subunits, and thus may confer in $Ca_v\beta_{1a}$ a specific ability to enter the nucleus. We created various truncation mutants of the $Ca_v\beta_{1a}$-YFP protein and tested their individual ability to enter the nucleus in the presence and absence of LMB (Fig. 3 A and Fig. S1). All constructs except for $Ca_V\beta_{1a}$161-524 (lacking N terminus and SH3 domains; Fig. 3 B) showed enriched nuclear localization after LMB treatment, including the mutant lacking the putative yeast NLS. Several constructs lacking the GK domain showed strong nuclear localization without LMB; however, this could be attributed to low molecular weight. One exception is $Ca_v\beta_{1a}$-101-274 (Fig. 3 C), which contains SH3 and middle regions, and has a predicted molecular weight (47 kD when fused to YFP) close to the 50-kD barrier. Overall, these data suggest that the nuclear localization domain of $Ca_v\beta_{1a}$ lies somewhere in the SH3 or middle region, in agreement with previous findings for other $Ca_V\beta$ subunits.

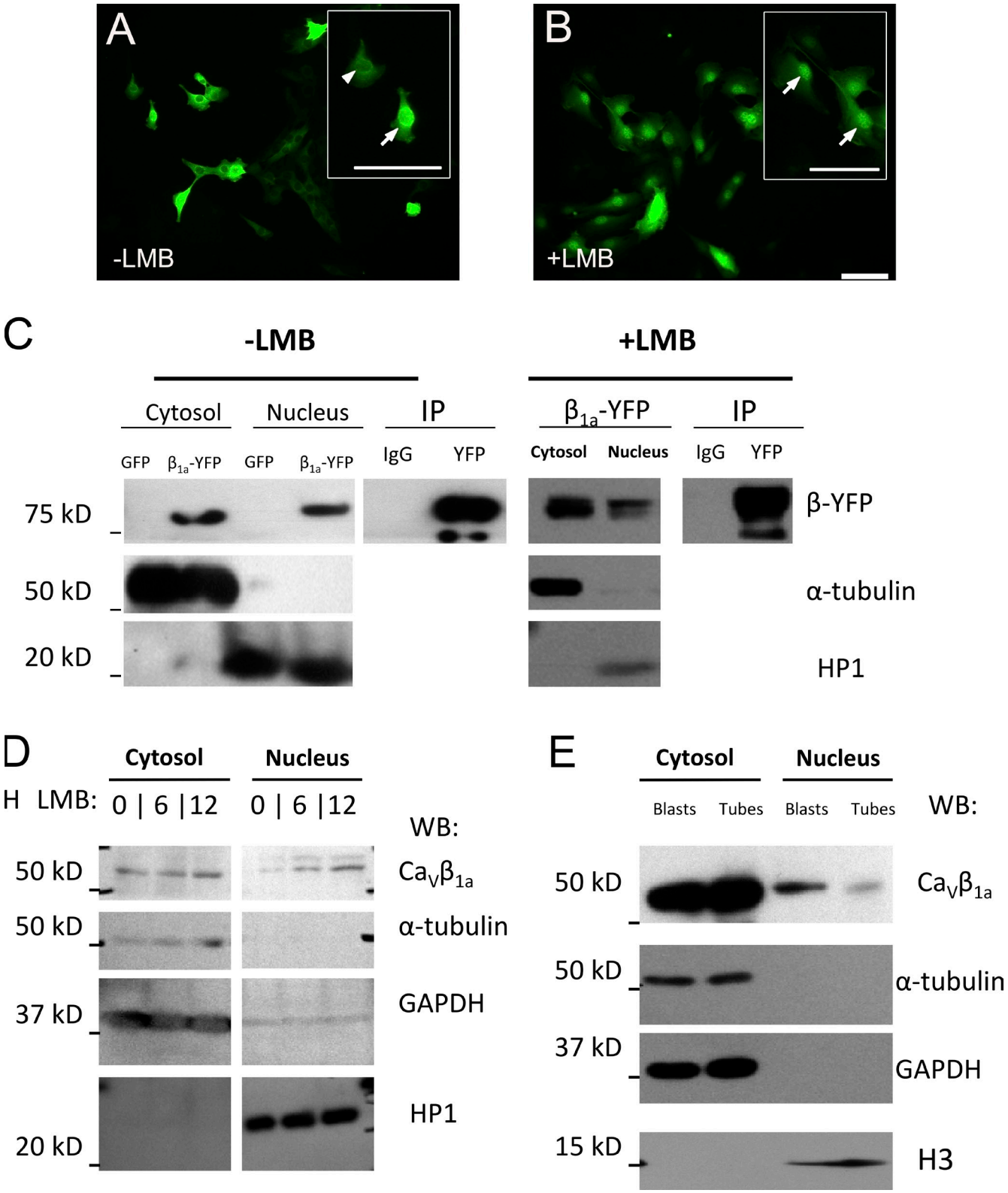

Figure 2. **$Ca_v\beta_{1a}$-YFP and endogenous $Ca_v\beta_{1a}$ translocate to the nucleus of myoblasts.** (A) C2C12 myoblasts transfected with $Ca_v\beta_{1a}$-YFP, and (B) after treatment with LMB. Arrowhead indicates cell with predominantly cytoplasmic $Ca_v\beta_{1a}$-YFP, arrows indicate cells with predominantly nuclear $Ca_v\beta_{1a}$-YFP. Bars, 100 µm. (C) Detection and immunoprecipitation of $Ca_v\beta_{1a}$-YFP in the nuclear fraction of untreated and LMB-treated C2C12 myoblasts by Western blot. (D) Western blot for endogenous $Ca_v\beta_{1a}$ in C2C12 myoblasts. Cytosolic and nuclear fractions of C2C12 myoblasts treated with LMB for 0, 6, and 12 h. (E) Comparison of $Ca_v\beta_{1a}$ protein levels in cytoplasmic and nuclear fractions in myoblasts vs. myotubes. Tubulin and GAPDH are cytosolic markers, and HP1 and H3 are nuclear proteins. Figures are representative of at least two independent experiments.

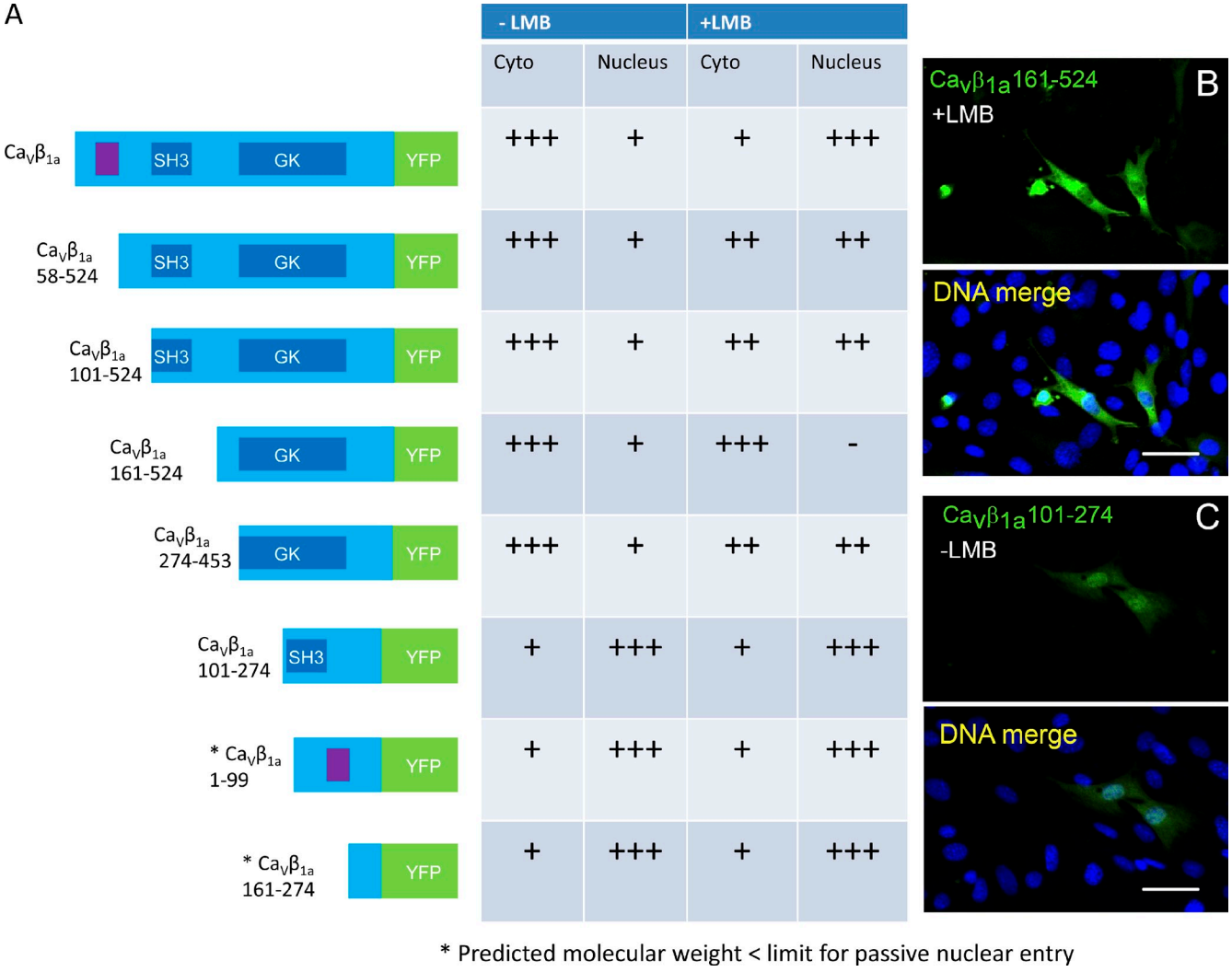

Figure 3. **Mapping of the $Ca_V\beta_{1a}$ nuclear localization domain.** (A) Diagram of constructed $Ca_V\beta_{1a}$-YFP truncation mutants and respective cytoplasmic and nuclear intensity in untreated and LMB-treated cells. Conserved SH3 and GK domains are noted in dark blue, putative NLS highlighted in purple, and YFP sequence in green. Construct names indicate amino acids remaining after truncation, with $Ca_V\beta_{1a}$-1-524 as full-length $Ca_V\beta_{1a}$. Table reflects relative intensity of cytoplasmic (Cyto) and nuclear $Ca_V\beta_{1a}$. (B) Enlarged image of $Ca_V\beta_{1a}$-161-524, which is absent from the nucleus after LMB treatment. (C) Enlarged image of $Ca_V\beta_{1a}$-101-274, which is present in the nucleus without LMB treatment. Nuclei (DNA) in all images were stained blue with Hoechst dye. Bars: (B and C) 50 µm.

Effects of altering $Ca_V\beta_{1a}$ expression on MPCs

Loss of the *Cacnb1* gene in mice leads to a noticeable deficit in muscle mass in prenatal stages (Gregg et al., 1996). Though this was attributed to lack of EC coupling in myofibers, we hypothesized it may be due in part to the loss of $Ca_V\beta_{1a}$ in MPCs as well. To test this, we examined the effects of knocking down $Ca_V\beta_{1a}$ on C2C12 myoblast proliferation in vitro. Because C2C12 myoblasts are not excitable and do not express $Ca_V1.1$ (Fig. 1 D; Bidaud et al., 2006), any effect from reduction of $Ca_V\beta_{1a}$ likely reflects a Ca_V-independent function of $Ca_V\beta_{1a}$. Stable transfection of cells with $Ca_V\beta_{1a}$ shRNA achieved substantial reduction of $Ca_V\beta_{1a}$ protein (Fig. 1 C). When observed in culture, $Ca_V\beta_{1a}$ shRNA-transfected cells grew more slowly than controls. To verify this observation, clonal cultures of scrambled control and $Ca_V\beta_{1a}$-shRNA–transfected C2C12 myoblasts were plated at equal densities and then counted 24 and 48 h later. Two out of three $Ca_V\beta_{1a}$-shRNA–transfected cultures showed significantly fewer cells at 24 and 48 h compared with scrambled controls (Fig. S2). Similarly, knockdown of $Ca_V\beta_{1a}$ in primary MPCs resulted in significantly impaired growth over 7 d in culture compared with controls, especially at later time points (Fig. 4 A). $Ca_V\beta_{1a}$ knockdown cells showed more frequent AnnexinV-FITC staining than control cells in vitro, although the difference was not significant ($P = 0.07$; Fig. S3 A). To further evaluate the role of $Ca_V\beta_{1a}$ in MPC proliferation, we cultured MPCs from E18.5 *Cacnb1*$^{-/-}$ embryos using FACS (Fig. S4 A). MPCs derived from *Cacnb1*$^{-/-}$ embryos also showed significantly less cell proliferation after 4 d in culture (Fig. 4 B) compared with heterozygous controls. Together, these data suggest that loss of $Ca_V\beta_{1a}$ expression severely affects MPC expansion.

MPCs are prone to spontaneous differentiation even under proliferative conditions; thus, we hypothesized that overexpression of $Ca_V\beta_{1a}$ may enhance proliferation in wild-type MPCs

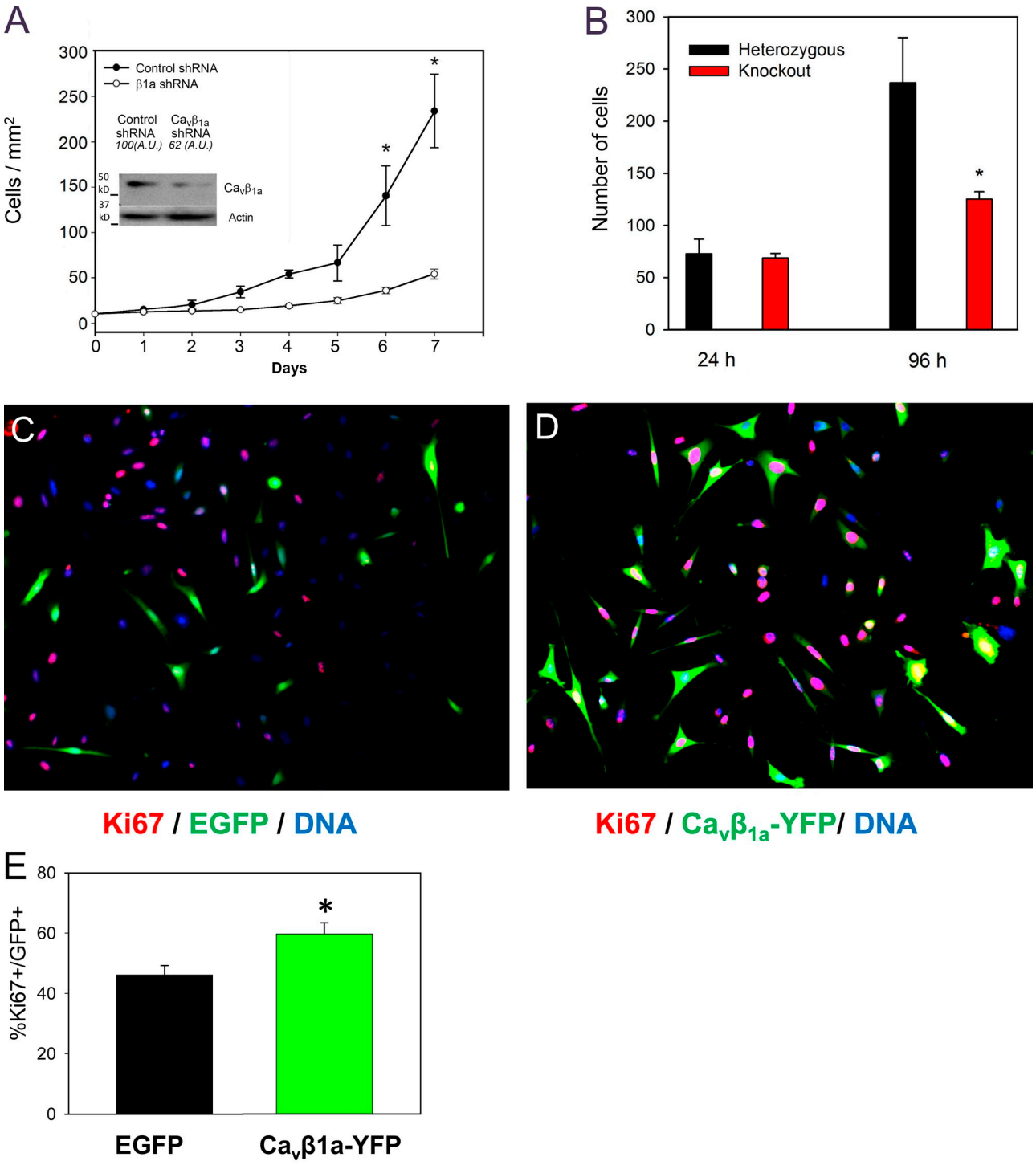

Figure 4. **Regulation of myoblast proliferation by $Ca_v\beta_{1a}$ in vitro and in vivo.** (A) Quantification of myoblast growth for 7 d after transfection with either scrambled control shRNA or $Ca_v\beta_{1a}$-targeted shRNA (Western blot of $Ca_v\beta_{1a}$ knockdown is inset). (B) Quantification of MPCs cultured from *Cacnb1*$^{+/-}$ and *Cacnb1*$^{-/-}$ embryos for 4 d (n = 4). (C–E) Primary mouse myoblasts transfected with EGFP (C) or $Ca_v\beta_{1a}$-YFP (D) and stained 24 h later for Ki67 (red; n = 3). Bar, 100 µm. (E) Quantification of Ki67+/EGFP and Ki67+/$Ca_v\beta_{1a}$-YFP cells expressed as a percentage of total EGFP or $Ca_v\beta_{1a}$-YFP + cells. *, $P < 0.05$.

by preventing differentiation. To test this idea, we transfected primary MPCs with an EGFP control plasmid (Fig. 4 C) or $Ca_v\beta_{1a}$-YFP (Fig. 4 D), and then stained for the marker of proliferation, Ki67 (Gerdes et al., 1984). After 24 h in culture, a significantly higher percentage of $Ca_v\beta_{1a}$-YFP–transfected cells were also Ki67 positive, compared with EGFP/Ki67-positive cells (Fig. 4 E). Thus, increasing $Ca_v\beta_{1a}$ expression level appears to enhance proliferation of MPCs, possibly by protecting against differentiation, further supporting the concept that $Ca_v\beta_{1a}$ plays a critical role in MPC expansion.

Due to the effects of $Ca_v\beta_{1a}$ loss on MPC proliferation in vitro, we hypothesized that some of the deficits in muscle mass

seen in *Cacnb1*$^{-/-}$ mice are due to impaired MPC proliferation, beyond the already known loss of $Ca_v1.1$ function and EC coupling. As *Cacnb1*$^{-/-}$ mice do not survive past birth, they must be studied at the embryonic stages. We chose to examine E13.5 embryos, as this time corresponds to the early stages of limb muscle development in mice, before complete innervation and large-scale muscle formation (Platzer, 1978; Ontell et al., 1995). Thus, effects from loss of EC coupling during development could be minimized, as most of the muscle cells at this time are newly formed myotubes or still in the progenitor phase. Hematoxylin and eosin (H&E) staining of hind limbs from E13.5 embryos showed that the relative area of nascent muscle bundles was markedly smaller in *Cacnb1*$^{-/-}$ embryos compared with wild type, whereas the overall number of the muscle bundles was similar (Fig. 5, A–C). Thus, the deficit in muscle mass previously observed in *Cacnb1*$^{-/-}$ mice (Gregg et al., 1996) occurs very early during muscle development. To test whether impaired MPC growth contributed to the lower muscle mass seen in *Cacnb1*$^{-/-}$ embryos, we stained cross sections of *Cacnb1*$^{+/+}$ (Fig. 5 D) and *Cacnb1*$^{-/-}$ (Fig. 5 F) hindlimbs for the MPC marker Pax7, and the proliferation marker Ki67. Compared with *Cacnb1*$^{+/+}$, *Cacnb1*$^{-/-}$ mice had a significantly lower number of Pax7$^+$ cells per μm^2 at the same time during development (Fig. 5 L). Surprisingly, the percentage of proliferating (Ki67$^+$) Pax7$^+$ cells was significantly higher in *Cacnb1*$^{-/-}$ embryos (Fig. 5 M), suggesting a possible compensatory mechanism by the remaining Pax7$^+$ MPCs. Importantly, this finding also indicates that loss of *Cacnb1* expression does not impair Pax7$^+$ MPC's ability to divide, per se, and therefore must limit the Pax7$^+$ MPC pool through more circuitous mechanisms. Accordingly, we measured AnnexinV-FITC/7AAD staining in E12.5 embryos by flow cytometry (Fig. S3 B) in order to see whether lower MPC numbers were due to increased rates of cell death on the preceding day. Similar to our in vitro results with $Ca_v\beta_{1a}$-shRNA in primary MPCs, *Cacnb1*$^{-/-}$ cells did not show an increase in any markers of apoptosis or necrosis. Next, we examined whether aberrant differentiation might explain reduced Pax7$^+$ MPC pool size by quantifying the number of myogenin (a marker of terminally differentiated skeletal muscle)-positive cells in E13.5 embryos (Fig. 5, H–L). *Cacnb1*$^{-/-}$ embryos had a comparable number of myogenin$^+$ cells to wild type, resulting in a higher ratio of myogenin$^+$/Pax7$^+$ cells (Fig. 5 N). The equal number of myogenin$^+$ cells juxtaposed with smaller Pax7$^+$ MPC pools suggests an increased preference for terminal differentiation in *Cacnb1*$^{-/-}$ embryos. Thus we conclude that loss of *Cacnb1* causes aberrant and/or premature terminal differentiation, which in turn leads to depleted Pax7$^+$ MPC pools and subsequently smaller muscle mass.

Chromatin binding of $Ca_v\beta_{1a}$

Our results demonstrate that $Ca_v\beta_{1a}$ enters the nucleus of myoblasts and loss of $Ca_v\beta_{1a}$ expression impairs MPC expansion. Therefore, we hypothesized that $Ca_v\beta_{1a}$ may act as a transcriptional regulator. To test this question, we performed chromatin immunoprecipitation (ChIP) on-chip assays (Fig. 6). A $Ca_v\beta_{1a}$ antibody was used to immunoprecipitate chromatin from C2C12 myoblasts, which was hybridized to promoter arrays containing 10-Kb coverage of 25,500 mouse genes at 35-bp resolution. Enriched $Ca_v\beta_{1a}$ binding was detected in the promoter regions of 952 genes (Table S3). Binding peaks were enriched closest to the transcription start site (TSS) of most genes (Fig. 6 A), with the vast majority falling inside or upstream of the gene-coding region (Fig. 6 B). Motif analysis revealed two highly enriched DNA sequences (Fig. 6 C). The first motif contains a noncanonical, heptameric E-box sequence (CANNNTG), which has been previously reported (Virolle et al., 2002). Several other motifs containing canonical (CANNTG) and noncanonical (CANNGG, CANNTT) E-box motifs were also enriched, although to a lesser degree. The second motif contains a Bicoid-class homeodomain sequence: TAATCC (Noyes et al., 2008). Functional annotation of enriched peaks revealed $Ca_v\beta_{1a}$ binds to the promoter regions of a broad set of genes, including many involved in signal transduction and stress response (Fig. 6 D). Normalized log2 ($Ca_v\beta_{1a}$/IgG) $Ca_v\beta_{1a}$-binding peaks at the promoter regions of genes of interest, namely transcription factors with known involvement in development, were visualized in the UCSC browser (Fig. 6 E). Secondary validation of these genes was tested by ChIP-PCR with a GFP/YFP antibody in untransfected and $Ca_v\beta_{1a}$-YFP–transfected myoblasts. Nearly all of the promoter regions tested showed greater than twofold enrichment, across multiple primer pairs, in the $Ca_v\beta_{1a}$-YFP–transfected cells, with the exception of negative controls (Fig. 6, F and G). Thus, $Ca_v\beta_{1a}$ localizes to the promoter region of numerous genes in separate experimental designs.

Global gene regulation by *Cacnb1*

To further complement our ChIP-on-chip data, we used microarray analysis to examine changes in global gene expression in the presence or absence of $Ca_v\beta_{1a}$. Pure MPC cultures were isolated from *Cacnb1*$^{+/+}$, *Cacnb1*$^{+/-}$, and *Cacnb1*$^{-/-}$ mice (Fig. S4), and total RNA was extracted and used from microarray analysis (Fig. 7 and Table S5). We identified genes of interest as those that showed significant fold change in a *Cacnb1* dose-dependent manner. Specifically, we identified 1,104 genes that decreased with decreasing *Cacnb1* expression (negatively regulated by *Cacnb1*; Fig. 7 A) and 1,888 genes that increased with decreasing *Cacnb1* expression (positively regulated by *Cacnb1*; Fig. 7 B). One gene negatively regulated by *Cacnb1* (increased in *Cacnb1*$^{-/-}$) of particular interest was the transcription factor myogenin (*Myog*). Myogenin is known to play a critical role in skeletal muscle development, and intriguingly was found in an increased ratio to Pax7$^+$ cells in our exploration of early muscle development in *Cacnb1*$^{-/-}$ embryos. Further functional analysis highlighted many genes involved in cell cycle regulation and muscle development (Fig. 7, A and B). Of the genes identified from ChIP-on-chip, 40 showed increased expression in *Cacnb1*$^{-/-}$ cells, whereas 70 showed decreased expression, indicating that $Ca_v\beta_{1a}$ may act as both a positive and negative regulator of gene expression at the chromatin level (Table S6).

Cacnb1 regulates *Myog*

Myogenin acts as a switch for MPCs to transition from proliferation to differentiation, and previous studies have shown that precocious expression of myogenin can lead to MPC pool depletion

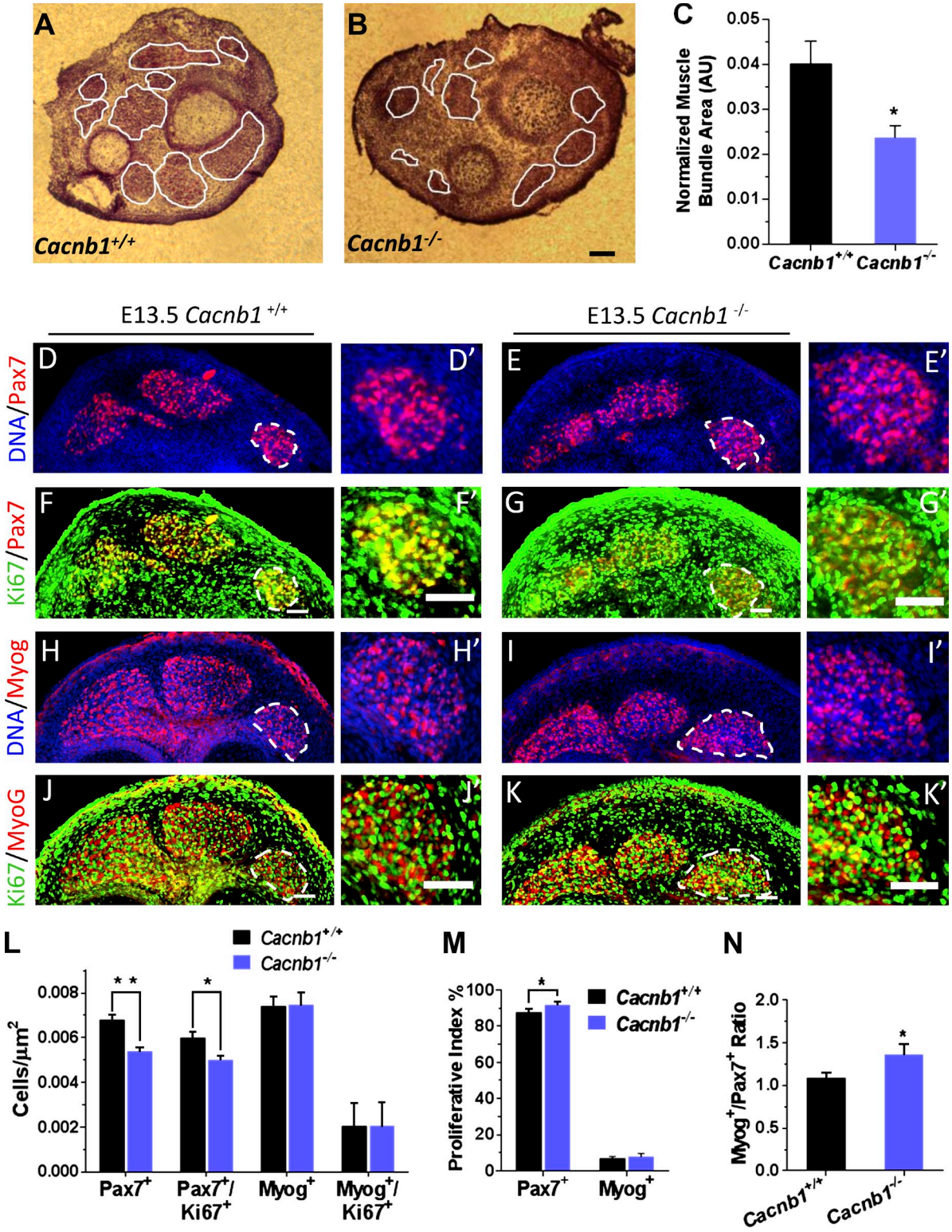

Figure 5. **Impaired skeletal muscle development in *Cacnb1*$^{-/-}$ mice.** (A–C) H&E staining of early muscle bundles in E13.5 *Cacnb1*$^{+/+}$ (A) and *Cacnb1*$^{-/-}$ (B) embryos (n = 3). Eosin positive bundles were traced, averaged, and normalized to overall cross section size (C). Bar, 100 µm. (D–N) Analysis of myogenic markers in *Cacnb1*$^{+/+}$ and *Cacnb1*$^{-/-}$ E13.5 embryos. Cross sections from *Cacnb1*$^{+/+}$ (D, F, H, and J) and *Cacnb1*$^{-/-}$ (E, G, I, and K) were stained for Pax7 (red) and Ki67 (green; D–G) or myogenin (red) and Ki67 (green; H–K). Nuclei (DNA) in all slides were stained blue with Hoechst dye. D′–K′ show magnified views of adjacent muscle bundles (dashed lines). Bars, 50 µm. (L) Quantification of absolute number of Pax7$^+$ and myogenin$^+$ cells, and absolute number of double-positive Pax7$^+$/Ki67$^+$ or myogenin$^+$/Ki67$^+$ cells, per µm^2. (M) Proliferative index as measured by percentage of Pax7$^+$ or myogenin$^+$ cells that were also Ki67$^+$. (N) Ratio of absolute number of myogenin$^+$ to Pax7$^+$ cells, per µm^2. n = 3 embryos each, 3 histological sections quantified per embryo. Data are mean ± SEM; *, $P < 0.05$; **, $P < 0.005$.

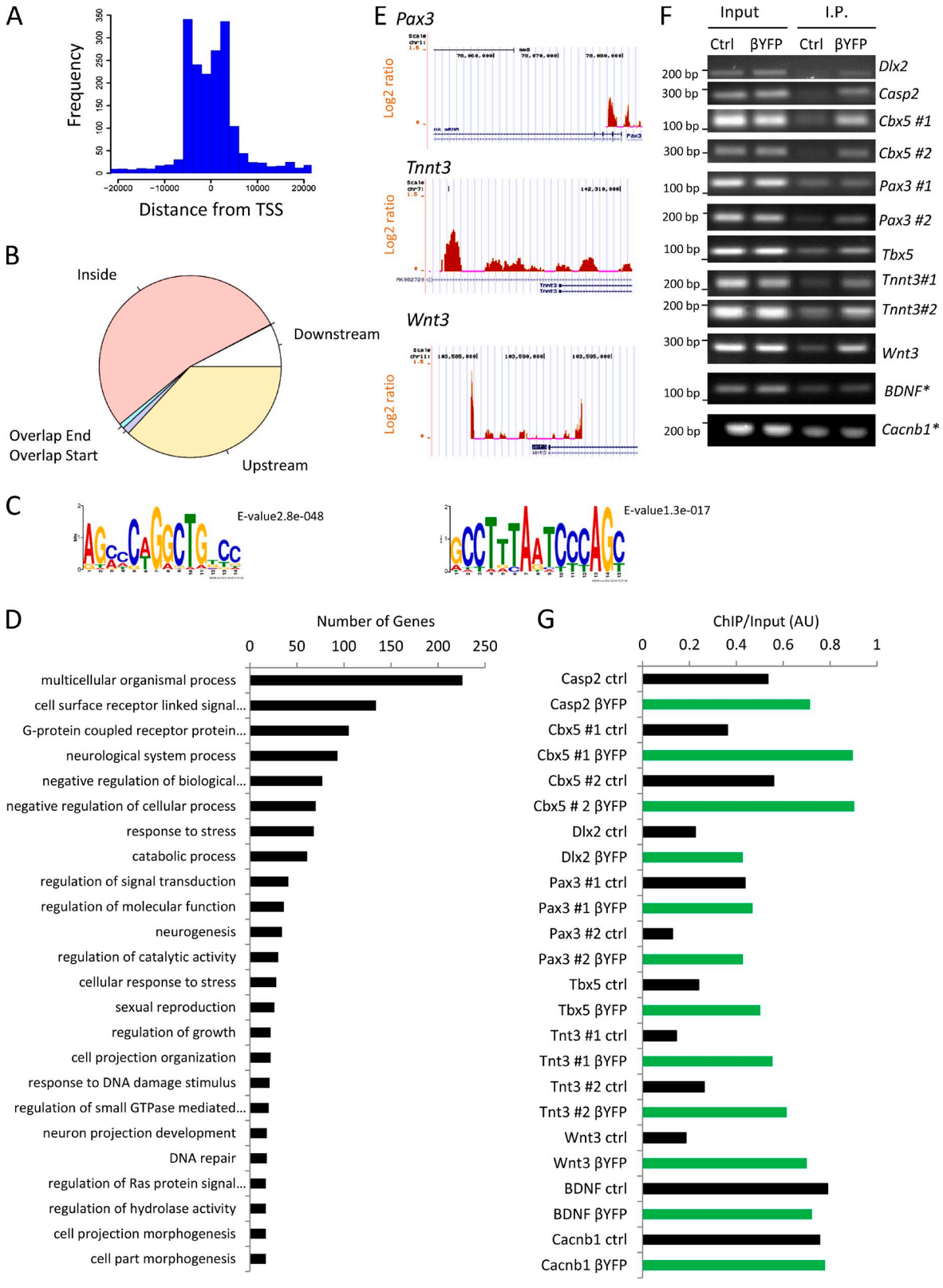

Figure 6. **ChIP-on-chip analysis of $Ca_v\beta_{1a}$.** (A) Histogram of $Ca_v\beta_{1a}$-binding distance from transcription start site. (B) Distribution of features of each $Ca_v\beta_{1a}$ peak relative to overlapping or nearest genes. (C) Top two consensus $Ca_v\beta_{1a}$ DNA-binding motifs. (D) Functional annotation of genes bound by $Ca_v\beta_{1a}$. Top 20 categories are shown. (E) Representative log2 ($Ca_v\beta_{1a}$/IgG) binding peaks on genes of interest in UCSC genome browser. Orange peaks indicate positive log2 $Ca_v\beta_{1a}$/IgG values and presumed sites of $Ca_v\beta_{1a}$ chromatin binding; blue indicates negative enrichment. (F and G) Validation of ChIP-chip–identified target genes by chromatin immunoprecipitation using a GFP antibody in control and $Ca_v\beta_{1a}$-YFP–transfected C2C12 myoblasts. "#" indicates separate primer pairs used to test multiple sites on each promoter region. Asterisk indicates negative controls. Immunoprecipitated DNA intensity was normalized to input for control and $Ca_v\beta_{1a}$-YFP (G).

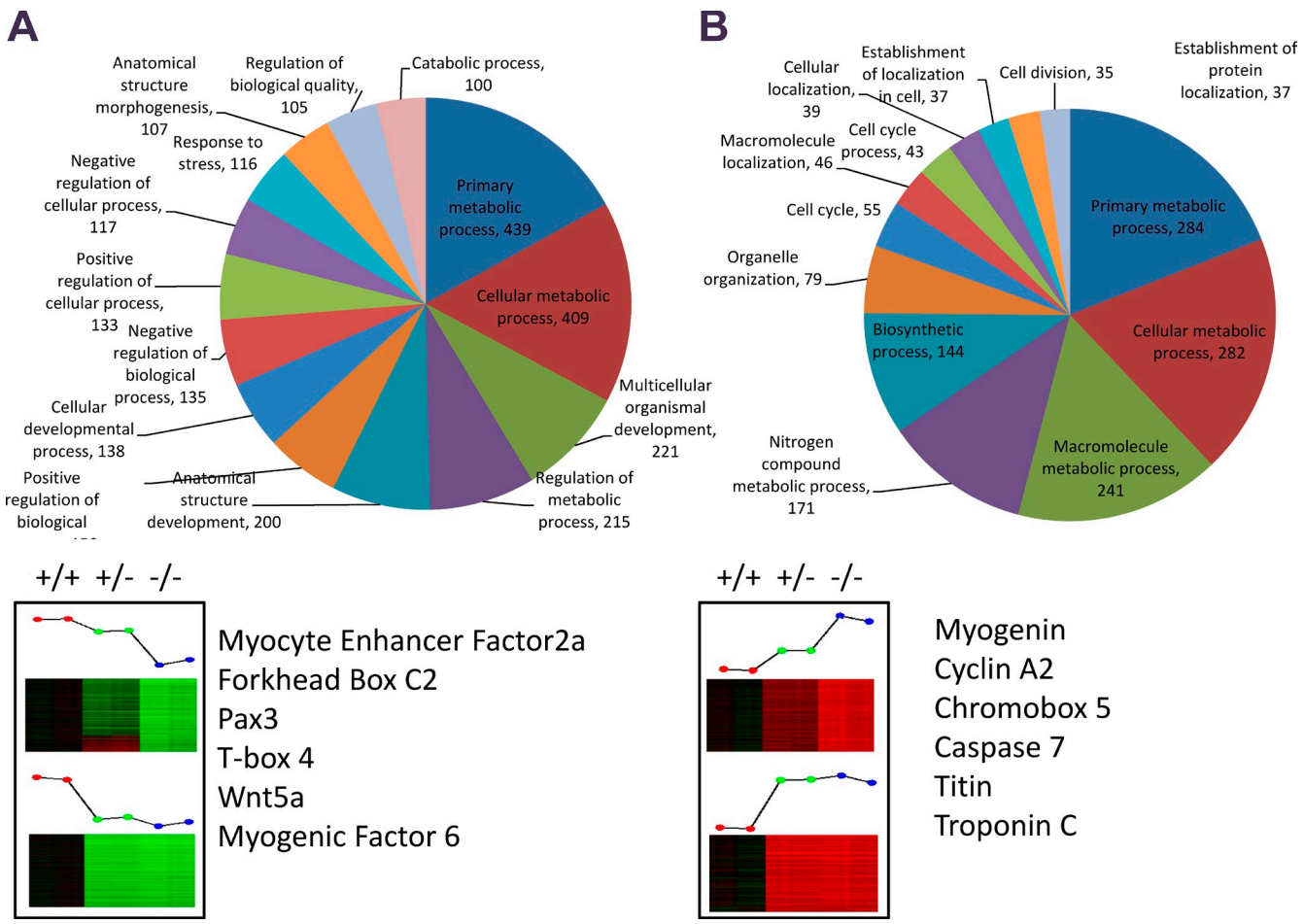

Figure 7. **Microarray analysis of *Cacnb1* wild-type (+/+), heterozygous (+/−), and knockout (−/−) MPCs.** Genes were selected based on dose-dependent correlation with *Cacnb1* expression. Genes said to be up-regulated by *Cacnb1* are lowest in −/− cells and functionally annotated in A, whereas genes said to be down-regulated by *Cacnb1* are highest in −/− cells and functionally annotated in B. GOTERM "other" (1,640 for A and 234 for B) was omitted from charts in order to improve visibility of other categories. Genes of interest involved in cell cycle and muscle development are listed below pie charts. See also Fig. S3 and Table S4.

(Schuster-Gossler et al., 2007; Van Ho et al., 2011). We therefore hypothesized that if *Myog* is inhibited by $Ca_v\beta_{1a}$, then the impaired MPC growth we observed when $Ca_v\beta_{1a}$ was knocked down/out was due to aberrant myogenin expression in these cells. To confirm our microarray results, we generated myogenic explant cultures from E18 embryos and quantified myogenin expression using immunocytochemistry (Fig. 8, A–C) and quantitative RT-PCR (Fig. 8 D). After 3 d, cultures from *Cacnb1*$^{-/-}$ embryos had significantly more myogenin-positive cells than *Cacnb1*$^{+/+}$ (Fig. 8 C). Myogenin mRNA was also approximately sevenfold higher overall in *Cacnb1*$^{-/-}$ cultures compared with *Cacnb1*$^{+/+}$ and *Cacnb1*$^{+/-}$ (Fig. 8 D). Similarly, primary MPC cultures transfected with $Ca_v\beta_{1a}$ shRNA showed a significantly higher percentage of myogenin-positive cells compared with controls (Fig. 8 E). To test whether loss of *Cacnb1* increases myogenin in MPCs in vivo, we measured myogenin mRNA in the hindlimb buds of E11.5 *Cacnb1*$^{+/+}$, *Cacnb1*$^{+/-}$, and *Cacnb1*$^{-/-}$ embryos (Fig. 8 F) at a time which predates differentiated muscle formation in the developing limb (Taher et al., 2011). Myogenin mRNA was ∼10-fold and 25-fold higher in the limb buds of *Cacnb1*$^{+/-}$ and *Cacnb1*$^{-/-}$ embryos, respectively, compared with wild-type controls. Together, these results demonstrate that loss of $Ca_v\beta_{1a}$ results in increased myogenin mRNA and protein, thus validating our microarray data, and also suggesting that $Ca_v\beta_{1a}$ acts to inhibit myogenin expression. To test whether this inhibition was dependent on $Ca_v\beta_{1a}$ nuclear entry, we used $Ca_v\beta_{1a}$-YFP mutants, which had shown the strongest and weakest nuclear localization (Fig. 3). Compared with full-length $Ca_v\beta_{1a}$-YFP, $Ca_v\beta_{1a}$-101-274-YFP (lacking GK domain and constitutively nuclear) showed an enhanced ability to suppress myogenin expression in differentiating C2C12 myoblasts, whereas $Ca_v\beta_{1a}$-161-524-YFP (lacking SH3 domain and constitutively cytoplasmic) was much less effective at inhibiting myogenin expression (Fig. 8 G).

We next sought to determine how $Ca_v\beta_{1a}$ regulates myogenin expression, hypothesizing that $Ca_v\beta_{1a}$ may interact with the *Myog* promoter. To initially test this idea, we made use of a luciferase reporter gene linked to a core region of the myogenin promoter (−184 +44; *Myog*-luc; Berkes et al., 2004). When *Myog*-luc–expressing C2C12 myoblasts were cotransfected with $Ca_v\beta_{1a}$-YFP, we saw decreased reporter gene activation compared with EGFP-transfected controls (Fig. 9 A), suggesting that $Ca_v\beta_{1a}$ represses myogenin gene expression via direct or indirect actions on the *Myog* promoter region. After two days in differentiation medium, $Ca_v\beta_{1a}$-YFP no longer suppressed *Myog*-luc

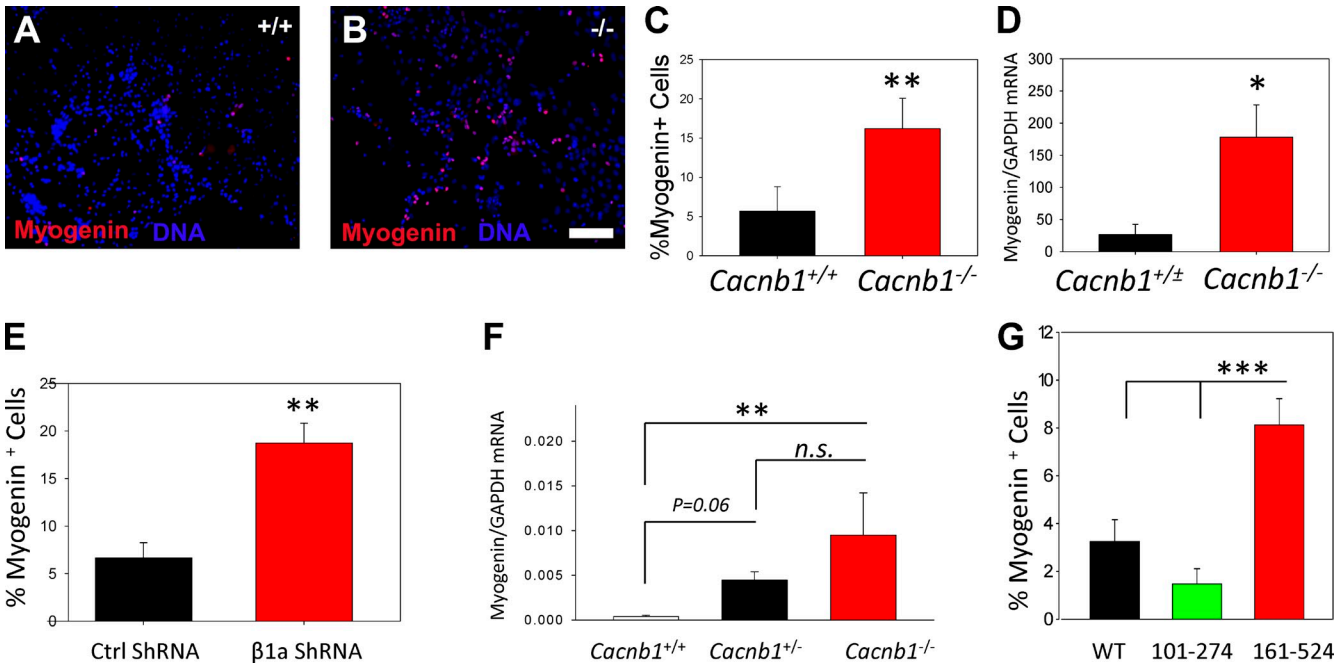

Figure 8. ***Cacnb1* modulates *Myog* expression in muscle progenitors.** Representative images from *Cacnb1*$^{+/+}$ (A) and *Cacnb1*$^{-/-}$ (B) E18.5 hindlimb explants cultures after 3 d in vitro. Bar, 100 µm. Cultures were then fixed and stained for myogenin (C; n = 5 and 3) or analyzed by quantitative PCR (D; n = 3 each, note that *Cacnb1*$^{+/+}$ and *Cacnb1*$^{+/-}$ are pooled). (E) Quantification of myogenin-positive cells in control and $Ca_v\beta_{1a}$-shRNA–treated primary MPC cultures (n = 3 each). (F) qPCR for myogenin mRNA from hindlimb buds dissected from *Cacnb1*$^{+/+}$, *Cacnb1*$^{+/-}$, and *Cacnb1*$^{-/-}$ E11.5 embryos (n = 6–12 each). (G) Quantification of myogenin expression in differentiating (1 d DM) C2C12 myoblasts, transfected with full-length, nuclear (101–274), or cytoplasmic (161–524) $Ca_v\beta_{1a}$ -YFP constructs (n = 6 each). Data are ± SEM; *, $P \le 0.05$; **, $P \le 0.01$; ***, $P \le 0.001$.

activity, indicating that the *Myog* promoter escapes $Ca_v\beta_{1a}$ regulation after terminal differentiation (Fig. 9 A). Conversely, C2C12 myoblasts cotransfected with *Myog*-luc and $Ca_v\beta_{1a}$ shRNA showed significantly higher luciferase activation than controls (Fig. 9 B). Thus, loss of $Ca_v\beta_{1a}$ protein enhances activation of the *Myog* promoter. In addition, ChIP-qPCR (Fig. 9 C) of $Ca_v\beta_{1a}$-YFP showed specific enrichment of the proximal *Myog* promoter, but not a region of intragenic DNA 3′ to the *Myog* gene. Although modest (approximately twofold), this level enrichment was comparable to $Ca_v\beta_{1a}$ binding at the *TnnT3* promoter region that we identified from our ChIP-on-chip experiments, versus another unbound region located in exon 5 of the *Cacnb1* gene (Fig. 9 C).

The proximal *Myog* promoter contains several conserved transcription factor–binding sites, leading us to examine which site(s) $Ca_v\beta_{1a}$ might act on within this region. Motif analysis from our ChIP-on-chip data led us to investigate both canonical and noncanonical E-boxes, and homeobox motifs within the core (−184 +44) *Myog* promoter. In electrophoretic mobility shift assays (EMSAs), addition of $Ca_v\beta_{1a}$-YFP protein caused a specific shift of a probe containing the NC E-box from our ChIP-on-chip consensus motif (9D). However, a probe containing the secondary homeodomain-binding motif (TAATCC) was not shifted by $Ca_v\beta_{1a}$-YFP. A probe from a portion of the *Myog* promoter containing both a homeodomain site (Pbx) and an adjacent NC E-box (CAGCTTA) similar to our consensus motif was shifted by $Ca_v\beta_{1a}$-YFP protein, and supershifted by addition of a GFP/YFP antibody. Importantly, the shift induced by $Ca_v\beta_{1a}$-YFP to the *Myog* promoter probe could be almost completely erased by using our ChIP-on-chip–identified NC E-box sequence as a competitor. Thus, $Ca_v\beta_{1a}$ appears to interact with a heptameric NC E-box motif located in the proximal *Myog* promoter, although the higher affinity of $Ca_v\beta_{1a}$-YFP for the *Myog* promoter sequence than for our consensus motif suggests this fragment of the Myog promoter may contain additional sequences important for $Ca_v\beta_{1a}$ binding. To better understand the relationship between $Ca_v\beta_{1a}$-YFP, canonical and noncanonical E-boxes, and homeodomain motifs, within the context of *Myog* promoter activity, we used *Myog*-luc mutant constructs (Berkes et al., 2004). Mutation of both canonical and noncanonical E-box motifs attenuated $Ca_v\beta_{1a}$-YFP–induced inhibition, whereas mutation of the homeodomain/Pbx-binding site actually enhanced inhibition by $Ca_v\beta_{1a}$-YFP (Fig. 9 E). We conclude that $Ca_v\beta_{1a}$ binds to the proximal Myog promoter at a specific NC E-box motif, and that its binding affinity may be regulated by complex involvement from nearby homeodomain and E-box sites.

Because of its apparent involvement with canonical and noncanonical E-box sites, as well as homeodomain sites, we tested the ability of $Ca_v\beta_{1a}$-YFP to interact with E-box and homeodomain proteins known to bind to the *Myog* E-box–binding proteins. MyoD (Cheng et al., 1992), Mef2 (Edmondson et al., 1992), and homeodomain proteins Lef-1 (not expressed in myoblasts; Fig. S5 A) and Pbx1 (Berkes et al., 2004) all failed to co-precipitate with $Ca_v\beta_{1a}$-YFP (Fig. S5 B). Expression of $Ca_v\beta_{1a}$-YFP did not alter the subnuclear localization of MyoD or Mef2 (Fig. S5 C), suggesting that $Ca_v\beta_{1a}$ does not act on the *Myog* promoter in concert with any of these proteins. Together, these results indicate that $Ca_v\beta_{1a}$ does not bind the *Myog* promoter as part of a complex with MyoD, Mef2, or Lef-1, suggesting an interaction with other proteins.

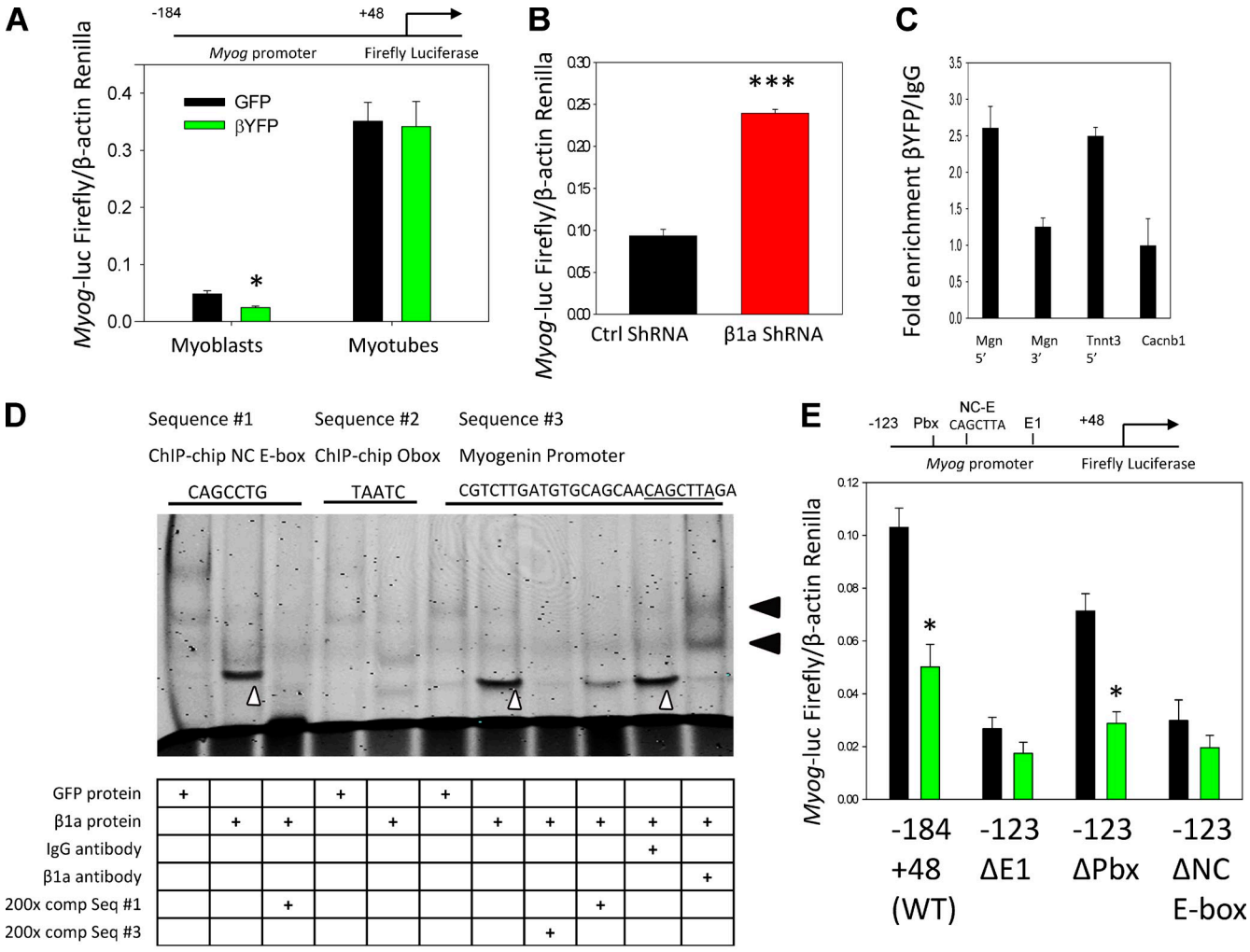

Figure 9. **$Ca_v\beta_{1a}$ action at the Myog promoter.** (A) *Myog*-luc expression in GFP (black) or $Ca_v\beta_{1a}$-YFP (green) expressing myoblasts (n = 5) and myotubes (n = 6). (B) *Myog*-luc expression in control (black) and $Ca_v\beta_{1a}$-shRNA (red)–transfected C2C12 myoblasts (n = 3). (C) ChIP-qPCR showing relative fold enrichment of $Ca_v\beta_{1a}$-YFP pull-down of *Myog* promoter (Mgn 5′) and *Tnnt3* promoter (*Tnnt3*), with *Myog* 3′ region (Mgn 3′) and *Cacnb1* exon 5 (*Cacnb1*) as controls. (D) Gel shift assay using GFP protein (control) or $Ca_v\beta_{1a}$-YFP protein from Cos7 nuclear extracts. Mouse IgG is nonspecific antibody. A specific shift can be seen in lanes 2, 7, and 10 (white carats), and supershift induced by YFP antibody seen in lane 11 (black arrowheads). Fluorescently labeled probe sequences (top) were generated from ChIP-chip motif results (sequences #1 and #2) and from the Myog promoter (sequence #3; NC E-box motif underlined). Full probe sequences are available in Table S1. (E) Mutation analysis of *Myog* promoter. C2C12 were transfected with GFP (black) or $Ca_v\beta_{1a}$-YFP (green) and then wild-type (−184 +48) *Myog*-luc, or −123 +48 fragments with mutations in E1 E-box (ΔE1), Pbx1 (ΔPbx), or noncanonical E-box (ΔNC E-box; CAGCTTA sequence indicated in D has been mutated to TGGCTTA) *Myog*-luc constructs, n = 3 per group. Locations of mutations are indicated above. See Berkes et al. (2004) for origin of these constructs. Data are ± SEM; *, $P \leq 0.05$; ***, $P \leq 0.001$.

Discussion

$Ca_v\beta_{1a}$ has long been known solely for its essential role in skeletal muscle EC coupling. Though a few reports have intimated roles for the protein as a transcriptional regulator, a well-defined physiological context for $Ca_v\beta$ subunits outside of Ca_v-regulation has yet to be established. Here we show that the $Ca_v\beta_{1a}$ subunit regulates skeletal muscle myogenesis in vivo during embryonic development via repressive actions on the *Myog* promoter in MPCs.

The idea of Ca_v-independent roles for $Ca_v\beta$ subunits has been suggested previously, which has been mainly tied to their nuclear translocation. $Ca_v\beta_{4c}$ and $Ca_v\beta_3$ subunits have been shown to regulate transcription in vitro by direct suppression of Hp1 (Hibino et al., 2003) and Pax6(s) (Zhang et al., 2010), respectively, in a Ca_v-independent fashion. A precise physiological role for Ca_v-independent functions of $Ca_v\beta$ subunits has been elusive, but a few recent clues have emerged. Garrity and colleagues have also shown effects of morpholino-mediated $Ca_v\beta$ knockdown in zebrafish models: knockdown of $Ca_v\beta_4$ prevented normal epiboly in early zebrafish embryos, which could be rescued by a Ca_v-binding–deficient mutant $Ca_v\beta_4$ (Ebert et al., 2008). Interestingly, this group also found impaired cardiac progenitor cell proliferation in 24–30 and 30–36 h post-fertilization zebrafish embryos after $Ca_v\beta_2$ knockdown (Chernyavskaya et al., 2012). The latter finding is especially compelling in the context of our findings that $Ca_v\beta_{1a}$ knockdown/gene knockout in muscle progenitor cells impairs their expansion in vitro and in vivo. $Ca_v\beta$ subunits may also have distinct nuclear functions in mitotic versus post-mitotic cells, as evidenced by recent papers showing

specific actions for $Ca_v\beta_4$ in the nucleus of cerebellar neurons (Subramanyam et al., 2009; Tadmouri et al., 2012). An interesting future direction will be to explore the potential nuclear role of $Ca_v\beta_{1a}$ in differentiated skeletal muscle.

A foundation of our study was the novel finding that $Ca_v\beta_{1a}$ enters the nucleus of MPCs. An important question that remains is how do $Ca_v\beta_{1a}$, and $Ca_v\beta$ subunits, in general, travel to the nucleus? One possibility is that $Ca_v\beta$ subunits bind to other proteins, either in a conserved or isoform/tissue-specific fashion. Earlier works with other $Ca_v\beta$ subunits offered several different protein-binding partners that may be responsible for their nuclear translocation, including the aforementioned Hp1 and Pax6(s) proteins, as well as the RGK (Rad, Rem, Gem/Kir) family of proteins (Buraei and Yang, 2010), and B56δ and PP2A (Tadmouri et al., 2012). In our own assays, neither Hp1 nor the RGK protein Rem coprecipitated with $Ca_v\beta_{1a}$-YFP (unpublished data). We also did not see evidence of $Ca_v\beta_{1a}$ interaction with Lef1 or several other proteins also known to regulate the *Myog* promoter (MyoD, Mef2, Pbx1), leaving this as an open question.

Another possibility is that $Ca_v\beta$ enters the nucleus based on an NLS specific to one or more isoforms of the protein. We believe this to be less likely, as $Ca_v\beta$ subunits do not possess a classical NLS, and truncation of a lysine/arginine-rich putative yeast NLS (Hicks and Raikhel, 1995) does not affect nuclear localization of our $Ca_v\beta_{1a}$-YFP constructs. Our work and other studies (Hibino et al., 2003; Takahashi et al., 2005) highlight the importance of the SH3 domain for $Ca_v\beta$ nuclear translocation. The apparent importance of the SH3 domain in nuclear localization across $Ca_v\beta$ isoforms suggests that this phenomenon is conserved, yet the individualized preference of $Ca_v\beta$ isoforms for nuclear binding partners paradoxically argues in favor of isoform-specific mechanisms of nuclear translocation. The SH3 domain contains a PxxP binding motif (Buraei and Yang, 2010), and may therefore bind multiple NLS-containing proteins in a tissue-specific fashion, offering a possible way to reconcile these findings.

Reduced skeletal muscle mass has been associated with loss of the *Cacnb1* gene since the original creation of the knockout mouse (Gregg et al., 1996). This phenotype was viewed as similar to that seen in the dysgenic ($Ca_v1.1$ mutant; Pai, 1965; Knudson et al., 1989; Chaudhari, 1992), and dyspedic (RyR mutant; Takeshima et al., 1994), and therefore attributed to lack of EC coupling during development. Although the initial report looked at mice in the late prenatal stage (E18), we observed deficits in *Cacnb1*$^{-/-}$ muscle mass as early as E13.5, suggesting a sustained impairment during early muscle development. We also observed fewer Pax7$^+$ MPCs in *Cacnb1*$^{-/-}$ hindlimbs, a deficit which cannot be explained by lack of EC coupling. Furthermore, myogenin mRNA was increased in the limb buds of E11.5 mutant mice, at a time that predates myotube formation (Taher et al., 2011) and thus EC coupling. It is possible that Ca_vs play some other role in MPC proliferation/expansion, beyond EC coupling. However, this appears unlikely, as our data from C2C12 myoblasts showed both the complete absence of $Ca_v1.1$ expression and the absence of $Ca_v\beta_{1a}$ membrane localization, together suggesting the total absence of any functional Ca_vs in MPCs. Additionally, a previous report found no differences in the growth rate of MPCs isolated from wild-type and dysgenic mice (Pinçon-Raymond et al., 1991).

A key concept in the field of skeletal muscle development and regeneration is the need for precise balance between progenitor cell proliferation and differentiation. Terminal differentiation (e.g., myogenin expression) of MPCs is closely associated with their exit from the cell cycle, recently underscored by work showing that myogenin promotes the expression of the anti–cell cycle miRNA20a (Liu et al., 2012). Therefore, suppression of differentiation proteins, such as myogenin, is critical for normal MPC expansion. Several works in mutant mouse models (Schuster-Gossler et al., 2007; Van Ho et al., 2011) show that a decreased number of Pax3/Pax7$^+$ MPCs during development is associated with an increase in myogenin$^+$, and presumably terminally differentiated cells. This is consistent with our findings that *Cacnb1*$^{-/-}$ mice show a higher ratio of myogenin$^+$/Pax7$^+$ MPCs in hindlimbs at E13.5, which is preceded by significantly higher myogenin mRNA in hindlimb buds at E11.5. Based on our data, we propose a mechanism for this pathway by which $Ca_v\beta_{1a}$ acts at the *Myog* promoter region to suppress its transcription (Fig. 10).

The question of exactly how $Ca_v\beta_{1a}$ regulates the *Myog* promoter is complex. Our ChIP-on-chip experiment did not identify *Myog* as a gene bound by $Ca_v\beta_{1a}$, yet our ChIP-qPCR and EMSA results indicated it was. A possible reconciliation for these findings is that $Ca_v\beta_{1a}$ binds weakly or transiently to *Myog* (in agreement with our relatively low ChIP-qPCR enrichment), and perhaps acts to displace or rearrange a larger protein complex. The primary DNA consensus motif discovered for $Ca_v\beta_{1a}$ was an NC (heptameric) E-box, followed by a Bicoid-class homeodomain motif. In addition, several hexameric NC E-boxes were identified (unpublished data). $Ca_v\beta_{1a}$-YFP bound to NC E-box sequences in EMSAs, but not homeodomain motifs, suggesting a selective association with E-box or NC E-boxes found adjacent to homeodomain sequences, while not acting directly on the homeodomain sequences themselves. The *Myog* promoter contains such an arrangement (Berkes et al., 2004), and EMSA and *Myog*-luc assays provided strong evidence that $Ca_v\beta_{1a}$ localizes and acts on this element of the *Myog* promoter.

It is important to note that whereas $Ca_v\beta_{1a}$ inhibits myogenin expression in MPCs, $Ca_v\beta_{1a}$ expression actually increases during myogenic differentiation in vitro, a period well known to be marked by a transient increase in myogenin expression. Therefore, under normal circumstances it seems that the *Myog* promoter finds a way to escape $Ca_v\beta_{1a}$-mediated inhibition during differentiation. The apparent decline in $Ca_v\beta_{1a}$ nuclear localization with myogenic differentiation offers a partial mechanism for this escape, although some visible $Ca_v\beta_{1a}$ apparently remains in the nucleus of differentiated myotubes, suggesting additional regulatory mechanisms. The identification of cofactors involved in $Ca_v\beta_{1a}$ regulation of the *Myog* promoter is critical for addressing this question.

Our work describes a highly novel role for $Ca_v\beta_{1a}$ in MPCs, from the molecular to physiological level. The specific function of $Ca_v\beta_{1a}$ in skeletal muscle and the generalized role (if any) for all $Ca_v\beta$ subunits in the nucleus are both important lines of research, and both should offer important insight into basic cellular function and human health and disease.

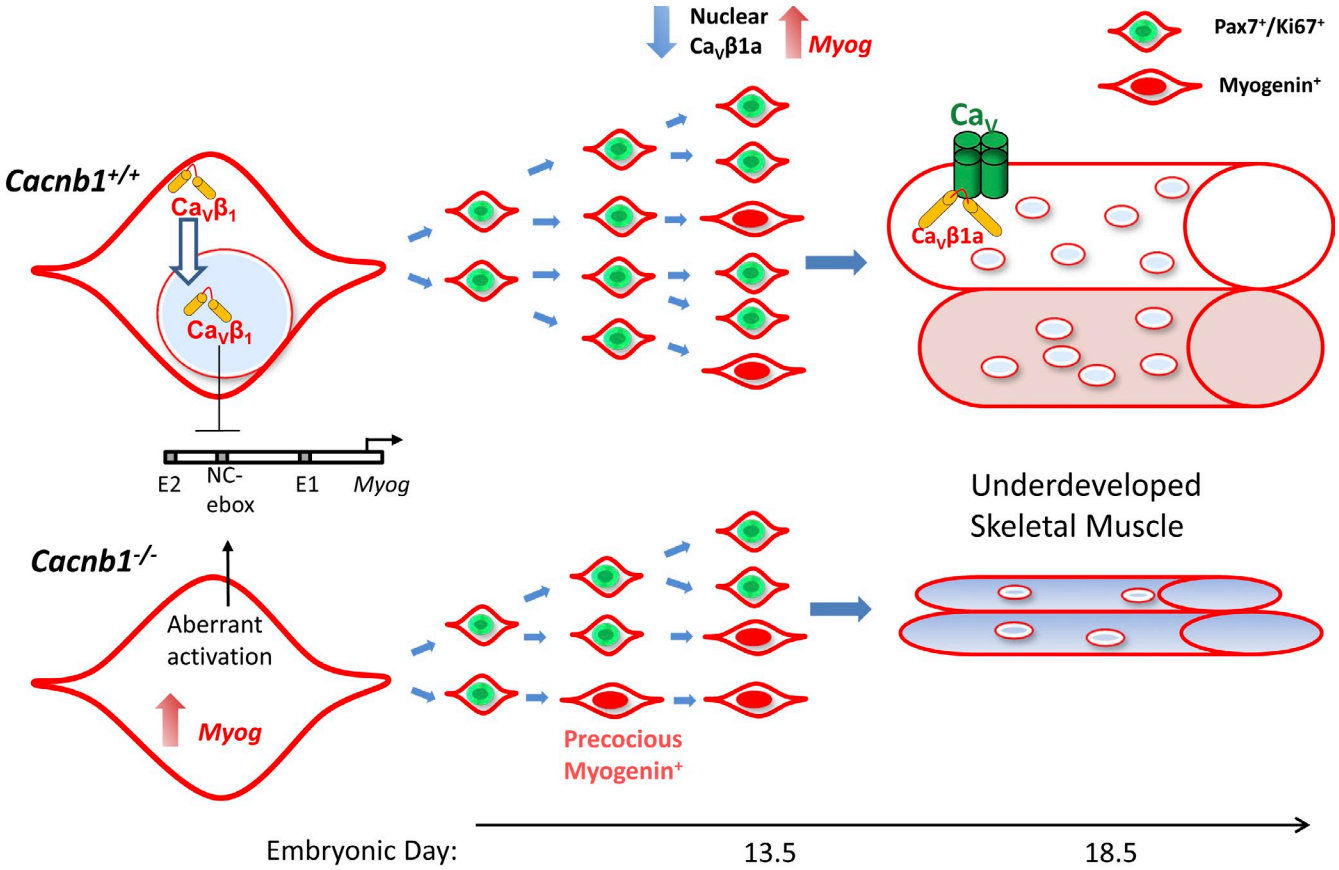

Figure 10. **Mechanism of Ca$_V$β$_{1a}$ regulation of myogenesis.** In *Cacnb1*$^{+/+}$ MPCs, Ca$_V$β$_{1a}$ enters the nucleus and acts on an NC E-box on the *Myog* promoter, suppressing *Myog* expression and allowing Pax7$^+$ MPCs to proliferate in sufficient quantity. Following differentiation cues, Ca$_V$β$_{1a}$ exits the nucleus and Myog is disinhibited, allowing terminal differentiation and fusion of myotubes. In *Cacnb1*$^{-/-}$ MPCs, *Myog* is not properly suppressed, leading to increased probability of *Myog* up-regulation and precocious differentiation. The number of myogenin-expressing cells is initially higher, but because their formation also depletes the Pax7$^+$ progenitor pool, there are fewer precursors to form myogenin-positive cells at later time points. The final result is underdeveloped skeletal muscle.

Materials and methods

RT-PCR and real-time PCR

Total RNA was isolated from cells and tissue using TRIzol reagent. Primer sequences used for RT-PCR and ChIP-PCR, as well as product numbers for real-time TaqMan primers (Applied Biosystems) are listed in Table S1. For real-time PCR, gene expression was determined using the $2^{-\Delta\Delta CT}$ method (Livak and Schmittgen, 2001). mRNA was primed with random hexamers and reverse transcribed with Reverse Transcription III (Invitrogen). RT-PCR was performed on a GeneAmp PCR System 3700 (Applied Biosystems) under the default parameters for 35 cycles. For real-time PCR, samples were prepared using TaqMan Gene Expression Master Mix (Applied Biosystems) and TaqMan probes (Table S1) on a qPCR system (Mx3000P; Agilent Technologies), using the default parameters for 35 cycles.

Protein isolation and Western blot

Cytosolic and membrane fractionation were based on previous protocols (Leung et al., 1987; Taylor et al., 2009). In brief, C2C12 cells were collected with a rubber scraper, rinsed in ice-cold PBS, and lysed in ice-cold buffer A (20 mM sodium pyrophosphate, 20 mM sodium phosphate monobasic, 1 mM $MgCl_2$, 0.5 mM EDTA, and 303 mM sucrose with complete protease inhibitor cocktail [Roche]) using a handheld glass homogenizer. Homogenate was centrifuged at 100,000 *g* for 90 min at 4°C in a rotor (model Ti 70i; Beckman Coulter). The supernatant was saved as the cytosolic fraction. The pellet was rinsed with ice-cold PBS and resuspended with a glass homogenizer in fresh digitonin buffer (1% digitonin [wt/vol], 185 mM KCl, 1.5 mM $CaCl_2$, and 10 mM Hepes, pH 7.4, with complete protease inhibitor cocktail) as the membrane fraction.

For cytosolic and nuclear fractions, C2C12 myoblasts were lysed in Ontell buffer (Washabaugh et al., 2007; 19 mM NaCl, 1.5 mM $MgCl_2$, 20 mM Hepes, pH 7.4, 1 mM DTT, 20% glycerol, and 0.1% Triton X-100; 300 µl buffer per 100 mg tissue) using 50–100 strokes of a glass homogenizer. Lysate was centrifuged at 1,000 *g* for 10 min at 4°C and supernatant was taken as cytosolic fraction. Pellet was rinsed twice in Ontell buffer, then resuspended in buffer 2 (0.5 M sucrose, 5 mM $MgCl_2$, 10 mM Tris, 1 mM DTT, and 0.6 M KCl) as the nuclear fraction.

Protein concentration was measured using Bradford or bicinchoninic protein assays with bovine serum albumin standards.

For Western blotting, proteins samples were mixed with 2× Laemmli buffer (2% SDS, 20% glycerol, 0.004% bromophenol blue, 0.125 M Tris, and 5% β-mercaptoethanol; Laemmli, 1970). Samples to be probed for Ca$_v$1.1 were loaded in 8 M Urea buffer (8 M Urea, 20% SDS, 50 mM Tris, 0.004% BPB, 2 M Thiourea, and 1 mM DTT), boiled at 95°C for 5 min, and separated by SDS-PAGE using 10% polyacrylamide gels with 4.5% stacking gels. Proteins were transferred to PVDF membranes and blotted using 5% nonfat dry milk in TBS + 0.02% Tween 20 for all antibody incubation steps. Proteins were visualized with ECL Plus (GE Healthcare).

Antibody clone, dilution, and product numbers are listed in Table S2.

Construction of recombinant adenoviral vector RAd-Ca$_v$β$_{1a}$-YFP

cDNA for Ca$_v$β$_{1a}$-EYFP (GenBank accession no. M25514.1, donated by K. Beam, Colorado State University, Fort Collins, CO; Leuranguer et al., 2006) was inserted into a RAd vector by a variant of the two-plasmid method (Hitt et al., 1998) using the AdMax plasmid kit (Microbix). cDNA coding for Ca$_v$β$_{1a}$-YFP was excised from plasmid Ca$_v$β$_{1a}$-YFP (with EcoR I and Hpa I at the 5′ and 3′ end, respectively) and inserted in the multiple cloning site (MCS) of shuttle pDC516 (one of the shuttle plasmids in the kit), which contains an expression cassette consisting of the mouse cytomegalovirus promoter (mCMV) and the simian virus 40 (SV40) polyadenylation signal, immediately upstream and downstream of the MCS, respectively. Downstream of

this cassette, pDC516 also contains an frt recognition site for the yeast FLP recombinase. The second plasmid of the kit, the genomic plasmid pBHGfrt(del)E1,3 FLP, consists of the entire genome of adenovirus 5 (Ad5), with deletions in the E1 and E3 regions. Upstream of the E1 deletion, pBHGfrt(del)E1,3 FLP contains an expression cassette for the gene for yeast FLP recombinase, and immediately downstream the E1 deletion there is an frt recognition site. Both plasmids were cotransfected in HEK293 cells, a line stably transfected with a portion of the Ad5 E1 genomic region. In cotransfected HEK293 cells, FLP recombinase is readily expressed and efficiently catalyzes the site-directed recombination of the expression cassettes of pDC516 into the left end of pBHGfrt(del)E1,3 FLP, thus generating the genome of the desired recombinant adenoviral vector, RAd-Cavβ1a-YFP. The newly generated RAd was rescued from HEK293 cell lysates, plaque purified, and then purified by ultracentrifugation in CsCl gradient and dialyzed. Final virus stock was titrated by a serial dilution plaque assay. RAd-GFP control was purchased from the UNC Vector Core Facility (University of North Carolina at Chapel Hill, Chapel Hill, NC).

Histology and immunofluorescent staining

Animal housing and procedures were approved by the Animal Care and Use Committee of Wake Forest Health Sciences. For timed embryo studies, breeding pairs were placed together overnight and separated the following morning. Pregnancy was confirmed by sustained weight gain over the next 10 days. Genotypes were confirmed by PCR. Hindlimbs from E13.5 embryos (n = 3 per genotype) were removed from the whole body and placed in disposable embedding molds containing cold PBS. Then, they were cryopreserved by sucrose gradient (0.25 M sucrose in PBS for 1 h, 0.5 M sucrose in PBS for 45 min, and finally 1.5 M sucrose in PBS for 30 min), embedded in tissue-freezing medium (Triangle Biomedical Sciences, Inc.), and frozen in dry ice–chilled isopentane. Tissue blocks were stored at −80°C until sectioning (modified from Le Grand et al., 2004). For immunofluorescent staining, cells and 12 µM transverse cryosections were fixed with 4% PFA in PBS and permeabilized with 0.3% Triton X-100 in PBST (0.05% Tween 20). Heat-induced epitope retrieval was performed in embryo sections for Pax7 antigen using a steam pressure–based system (2100 Retriever; PickCell Laboratories) and a modified citrate buffer commercially available (R-Buffer A; Electron Microscopy Sciences). Once the retrieval cycle was completed, the slides were allowed to cool down inside the machine for at least 40 min. After antigen retrieval, slides were rinsed with PBST, blocked in 5% goat serum for 1 h at room temperature, and incubated overnight with primary antibodies at 4°C (see Table S2). Because both anti-Pax7 and anti-myogenin antibodies derived from a mouse host equivalent/analogous slides were chosen for each hindlimb and staining was performed separately for these antigens. Anti-Ki67 and nuclear staining (Hoechst) were included in every case. Slides were mounted with fluorescent mounting medium (Dako). Hematoxylin Gill no. 2 and Eosin Y (Sigma-Aldrich) solutions were used for H&E staining, and slides were mounted with Cytoseal (Thermo Fisher Scientific). LMB (LC Laboratories) was added to culture medium at 20 nM for 3 h before fixation or lysate collection. For the E13.5 embryo immunostaining, one hindlimb of each subject was sectioned in order to completely span the region between the future knee and ankle. The tibia and fibula were used as reference to identify the tibialis anterior, extensor digitorum longus, and peroneus brevis/longus developing muscles. A total of three sections per hindlimb containing these three muscle bundles were analyzed for every combination of antigens. Images were captured on a microscope (IX81; Olympus) with an Orca TC^2 camera (Hamamatsu Photonics) at room temperature and analyzed using MetaMorph Basic software. Objective lenses used were: UPLFLN 10× 2PH; U PLAN FL 10× Phase OBJ, NA 0.3; IPLSAPO 20×; U PLAN S-APO 20×, NA 0.75 (Olympus). Each bundle perimeter was delimited based on discreet clusters of Pax7 or myogenin staining and the area was calculated. The number of Pax7$^+$ and myogenin$^+$ nuclei within was determined using MetaMorph. Co-labeling of Pax7 or myogenin and Ki67 was determined by additive image overlay in the same software. All counting experiments were performed with the operator blind to experimental conditions.

Cell death analysis and flow cytometry

Cells were isolated from hindlimbs of E12.5 embryos by enzymatic digestion, pre-plated for 1 h on plastic, and stained for AnnexinV-FITC and 7AAD for 15 min at room temperature. Flow cytometry was performed on a flow cytometer (Accuri B6; BD).

Molecular cloning

$Ca_v\beta_{1a}$-YFP truncation mutants were cloned by PCR using primer pairs containing EcoR1 and SalI restriction enzyme digest sequences (listed in Table S1) and inserted into the pEYFP_n1 vector (Takara Bio Inc.). Sequencing confirmed all constructs (DNA Sequencing Laboratory, Wake Forest University Health Sciences [WFUHS]).

Fluorescence-activated cell sorting (FACS), primary cell culture, and transfection

C2C12 (ATCC) myoblasts were maintained in Dulbecco's modified essential medium (DMEM) with 10% fetal bovine serum (FBS). FACS was performed as described previously (Griffin et al., 2010) in a FACSAria (BD). Embryos were harvested at E18.5 under sterile conditions. Skeletal muscle was dissected from the limbs, minced, washed in ice-cold PBS, and incubated in a collagenase type II/dispase I solution for 1 h at 37°C. Cells were then triturated, passed through a 40-µm nylon mesh filter, washed, and labeled with α7-integrin APC and CD31/CD45-FITC–conjugated antibodies in PBS with 1% FBS for 30 min at 4°C and washed twice before FACS. MPCs were cultured on laminin (Invitrogen)-coated dishes in Ham's F10 medium with 20% FBS and basic FGF (5 ng/ml, Promega; Rando and Blau, 1994). Differentiation was induced upon C2C12 myoblasts or MPCs reaching 90% confluence by placing cells in DMEM with 2% horse serum. Lipofectamine 2000 (Invitrogen) was used for transfection. 5 $Ca_v\beta_{1a}$-specific shRNA sequences from the RNAi Consortium (Open Biosystems) were individually tested in C2C12 myoblasts selected with 3 ng/µl puromycin (Sigma-Aldrich). TRC 69052 showed the highest efficacy of $Ca_v\beta_{1a}$ protein knockdown and was used for further experiments. MISSION SHC002 nontargeting shRNA (Sigma-Aldrich) was used as a control. Explant cultures were prepared from E18.5 mice as described previously (Smith and Merrick, 2010). In brief, hindlimb muscles were dissected and cut into roughly 1-mm^3 cubes, which were then placed in 96-well culture dishes with growth medium for 3 d.

Microarray

Total RNA was prepared from FACS-sorted primary *Cacnb1* +/+, +/−, and −/− MPCs and hybridized to GeneChip Mouse Genome 430A 2.0 arrays (Affymetrix) according to manufacturer's instructions at the WFUHS Microarray Core Laboratory. CEL files were analyzed using Partek Genomics Suite (Partek) and grouped into nine categories of expression based on fold change between the three experimental groups. Functional annotation was performed using DAVID v6.7 software using GOTERM_BP_2 (Huang et al., 2009).

Luciferase assay

C2C12 myoblasts were infected with RAd $Ca_v\beta_{1a}$-YFP or RAd-GFP and 24 h later transfected with pMyog-firefly luciferase (a gift from S. Tapscott, Fred Hutchinson Cancer Research Center, Seattle, WA; Berkes et al., 2004) and β-actin–Renilla luciferase. Cells were checked for equal density and viral transfection and harvested 12 h later at confluence in GM, or after 48 h in DM, and normalized firefly to Renilla luciferase activity was measured using the Dual Luciferase Reporter Assay system (Promega).

ChIP-on-chip and ChIP-PCR/qPCR

Chromatin was immunoprecipitated from subconfluent C2C12 myoblasts using a $Ca_v\beta_{1a}$ antibody (H-50; Santa Cruz Biotechnology, Inc.) or control rabbit IgG (Santa Cruz Biotechnology, Inc.), hybridized to GeneChip mouse promoter 1.0R arrays (Affymetrix) according to the manufacturer's protocol. For ChIP buffer recipes, see Table S3. In brief, 5 × 10^7 C2C12 myoblasts were fixed in formaldehyde at a final concentration of 1% for 10 min, quenched with 2.5 M glycine, washed with PBS, and collected with a rubber cell scraper. The pellet was washed three times in lysis buffer, resuspended in Pre-IP dilution buffer, and sonicated for 10 × 60 s on ice. Average chromatin fragment size was confirmed on an agarose gel to be 200–1,000 bp before proceeding. Chromatin was precleared with protein A–Sepharose beads, then incubated overnight with antibodies at 4°C. The next day, chromatin was incubated with protein A–Sepharose beads for 4 h at room temperature. Beads were pelleted and washed with ChIP washes 1 and 2 (twice each for 5 min), ChIP wash 3, TE, and finally chromatin was eluted twice with elution buffer at 65°C. Cross-linking was reversed by incubation with proteinase K overnight at 65°C, and DNA purified using cDNA Cleanup Columns (Affymetrix). DNA was randomly primed using Sequenase and primer A (GTTTCCCAGTCACGGTC(N)^9; HPLC purified) and amplified using primer B (GTTTCCCAGTCACGGTC) and Taq polymerase. Amplification of fragments sized 200–2,000 bp was confirmed on an agarose gel. Samples were purified on a GeneChip Sample Cleanup Module (GE Healthcare). For ChIP-on-chip, DNA was fragmented, labeled, and hybridized to mouse promoter 1.0R arrays (Affymetrix) according to the manufacturer's protocol.

ChIP-PCR/qPCR

ChIP-PCR/qPCR was performed using an anti-GFP antibody (see Table S2) for immunoprecipitation, following the same protocol used for ChIP-on-chip.

Primers were designed using NCBI Primer-BLAST. ChIP-PCR was performed on a GeneAmp PCR System 3700 (Applied Biosystems) under the default parameters for 35 cycles. ChIP-qPCR was performed on a qPCR system (Mx3000P; Agilent Technologies), using the default parameters for 40 cycles.

EMSA

Nuclear protein extracts were prepared from Cos7 cells (Holden and Tacon, 2011), expressing either GFP or $Ca_v\beta_{1a}$-YFP, and incubated with infrared dye–labeled oligos (see Table S1) for 30 min at room temperature, and an additional 30 min with antisera or an equivalent volume of PBS. Samples were run on 4–12% nondenaturing TBE gels.

ChIP-on-chip analysis

The average log2 ($Ca_v\beta_{1a}$/IgG) intensity value of the two biological replicates was computed for each probe position. Regions enriched for $Ca_v\beta_{1a}$ relative to IgG were determined using CMARRT (Kuan et al., 2008) on the average log2 ($Ca_v\beta_{1a}$/IgG) at the FDR level of 0.05. Peak annotation, distance to TSS, and position to nearest gene were performed using ChIPpeakAnno (Zhu et al., 2010) and the Galaxy web platform (Blankenberg et al., 2010; Goecks et al., 2010). Refseq ID conversion to gene names and functional annotation were performed using DAVID v6.7 GOTERM_BP_ALL (Huang et al., 2009). For distance to TSS and peak position relative to nearest gene, peak coordinates were lifted over from mm8 to mm9 and then mapped to either the nearest or overlapping genes using the prebuilt transcription start sites annotation library for mouse genome TSS.mouse.NCBIM37. Peaks (log2 $Ca_v\beta_{1a}$/IgG intensity) were visualized in BedGraph format using the UCSC Genome Browser (Kent et al., 2002; University of California Santa Cruz, Santa Cruz, CA). Motif analysis was performed with MEME software (Bailey et al., 2009) and TOMTOM (Gupta et al., 2007).

For peak position, peaks not overlapping with a gene were tied to the nearest feature when generating the pie chart. "Overlap Start" and "Overlap End" correspond to peaks that overlap with gene transcription start and end site, respectively. "Upstream" and "Downstream" correspond to peaks that are upstream of gene transcription start site and downstream of gene transcription end site, respectively. "Inside" corresponds to peaks that are within gene region. "Inside" corresponds to peaks that cover the entire gene (especially for very short genes).

Data analysis

Data are presented as means ± SEM. Data were analyzed using SigmaPlot v11.0 with Student's *t* test or one-way ANOVA repeated measures, with Holm-Sidak test applied post hoc when appropriate. An α-value of $P < 0.05$ was considered significant.

Online supplemental material

Fig. S1 shows representative images of all $Ca_v\beta_{1a}$-YFP mutants with and without LMB treatment. Fig. S2 shows the effect of shRNA-mediated knockdown of $Ca_v\beta_{1a}$ in myoblast expansion in vitro. Fig. S3 shows the analysis of cell death in $Ca_v\beta_{1a}$ knockdown and *Cacnb1*$^{-/-}$ cells. Fig. S4 shows isolation strategy of muscle precursor cells from E18.5 embryos using FACS. Fig. S5 shows the screening for $Ca_v\beta_{1a}$-binding partners at the *Myog* promoter using Co-immunoprecipitation and fluorescent colocalization. Table S1 lists the primers used throughout the paper for various functions (RT-PCR, cloning, shRNA, etc.). Table S2 lists the antibodies used throughout the paper for various experiments (Western blot, immunocytochemistry, immunohistochemistry, ChIP). Supplier, clone, antigen, host, and dilutions are included. Table S3 lists the buffers used in ChIP. Table S4 is a complete list of genes with promoter regions found to be enriched for $Ca_v\beta_{1a}$ binding, and is related to Fig. 6 of the main text. Table S5 is a complete list of genes found to be differentially regulated by microarray analysis, between our three experimental groups. Genes are subdivided into the nine different patterns shown in Fig. S3. Table S5 is related to Fig. 7 of the main text. Table S6 displays a list of genes with promoter regions found to be ChIP enriched for $Ca_v\beta_{1a}$ binding and also showing differential regulation in expression by microarray analysis; subdivided into ChIP-enriched genes that are up-regulated in *Cacnb1*$^{-/-}$ (left-hand column) and ChIP-enriched genes that are down-regulated in *Cacnb1*$^{-/-}$ (right hand column). Online supplemental material is available at http:// www.jcb.org/cgi/content/full/jcb.201403021/DC1.

We would like to thank Dr. Ronald Gregg and Dr. Weichun Lin for developing and providing the *Cacnb1*$^{-/-}$ mice; Dr. Jeff Chou, Dr. Lance Miller, and Lou Craddock from the Wake Forest Baptist Health Microarray Core Facility; and James Wood and Beth Hollbrook from the Wake Forest Baptist Health Flow Cytometry Core.

This work was supported by NIH/NIA grants R01AG15820, R01AG13934, F31AG039934, and T32AG033534; and the Translational Sciences Institute at Wake Forest Baptist Health.

The authors declare no competing financial interests.

Submitted: 6 March 2014
Accepted: 16 May 2014

References

Bailey, T.L., M. Boden, F.A. Buske, M. Frith, C.E. Grant, L. Clementi, J. Ren, W.W. Li, and W.S. Noble. 2009. MEME SUITE: tools for motif discovery and searching. *Nucleic Acids Res.* **37**(Web Server, Web Server issue):W202–W208. http://dx.doi.org/10.1093/nar/gkp335

Béguin, P., K. Nagashima, T. Gonoi, T. Shibasaki, K. Takahashi, Y. Kashima, N. Ozaki, K. Geering, T. Iwanaga, and S. Seino. 2001. Regulation of Ca2+ channel expression at the cell surface by the small G-protein kir/Gem. *Nature*. 411:701–706. http://dx.doi.org/10.1038/35079621

Béguin, P., R.N. Mahalakshmi, K. Nagashima, D.H. Cher, H. Ikeda, Y. Yamada, Y. Seino, and W. Hunziker. 2006. Nuclear sequestration of beta-subunits by Rad and Rem is controlled by 14-3-3 and calmodulin and reveals a novel mechanism for Ca2+ channel regulation. *J. Mol. Biol.* 355:34–46. http://dx.doi.org/10.1016/j.jmb.2005.10.013

Berkes, C.A., D.A. Bergstrom, B.H. Penn, K.J. Seaver, P.S. Knoepfler, and S.J. Tapscott. 2004. Pbx marks genes for activation by MyoD indicating a role for a homeodomain protein in establishing myogenic potential. *Mol. Cell*. 14:465–477. http://dx.doi.org/10.1016/S1097-2765(04)00260-6

Bichet, D., V. Cornet, S. Geib, E. Carlier, S. Volsen, T. Hoshi, Y. Mori, and M. De Waard. 2000. The I-II loop of the Ca2+ channel alpha1 subunit contains an endoplasmic reticulum retention signal antagonized by the beta subunit. *Neuron*. 25:177–190. http://dx.doi.org/10.1016/S0896-6273(00)80881-8

Bidaud, I., A. Monteil, J. Nargeot, and P. Lory. 2006. Properties and role of voltage-dependent calcium channels during mouse skeletal muscle differentiation. *J. Muscle Res. Cell Motil.* 27:75–81. http://dx.doi.org/10.1007/s10974-006-9058-5

Blankenberg, D., G. Von Kuster, N. Coraor, G. Ananda, R. Lazarus, M. Mangan, A. Nekrutenko, and J. Taylor. 2010. Galaxy: a web-based genome analysis tool for experimentalists. *Curr. Protoc. Mol. Biol*. Chapter 19:Unit 19.10. 1–21.

Buraei, Z., and J. Yang. 2010. The ß subunit of voltage-gated Ca2+ channels. *Physiol. Rev.* 90:1461–1506. http://dx.doi.org/10.1152/physrev.00057.2009

Catalucci, D., D.H. Zhang, J. DeSantiago, F. Aimond, G. Barbara, J. Chemin, D. Bonci, E. Picht, F. Rusconi, N.D. Dalton, et al. 2009. Akt regulates L-type Ca2+ channel activity by modulating Cavalpha1 protein stability. *J. Cell Biol.* 184:923–933. http://dx.doi.org/10.1083/jcb.200805063

Chaudhari, N. 1992. A single nucleotide deletion in the skeletal muscle-specific calcium channel transcript of muscular dysgenesis (mdg) mice. *J. Biol. Chem.* 267:25636–25639.

Cheng, T.C., T.A. Hanley, J. Mudd, J.P. Merlie, and E.N. Olson. 1992. Mapping of myogenin transcription during embryogenesis using transgenes linked to the myogenin control region. *J. Cell Biol.* 119:1649–1656. http://dx.doi.org/10.1083/jcb.119.6.1649

Chernyavskaya, Y., A.M. Ebert, E. Milligan, and D.M. Garrity. 2012. Voltage-gated calcium channel CACNB2 (β2.1) protein is required in the heart for control of cell proliferation and heart tube integrity. *Dev. Dyn.* 241:648–662. http://dx.doi.org/10.1002/dvdy.23746

Colecraft, H.M., B. Alseikhan, S.X. Takahashi, D. Chaudhuri, S. Mittman, V. Yegnasubramanian, R.S. Alvania, D.C. Johns, E. Marbán, and D.T. Yue. 2002. Novel functional properties of Ca(2+) channel beta subunits revealed by their expression in adult rat heart cells. *J. Physiol.* 541:435–452. http://dx.doi.org/10.1113/jphysiol.2002.018515

Curtis, B.M., and W.A. Catterall. 1984. Purification of the calcium antagonist receptor of the voltage-sensitive calcium channel from skeletal muscle transverse tubules. *Biochemistry*. 23:2113–2118. http://dx.doi.org/10.1021/bi00305a001

Ebert, A.M., C.A. McAnelly, A. Srinivasan, J.L. Linker, W.A. Horne, and D.M. Garrity. 2008. Ca2+ channel-independent requirement for MAGUK family CACNB4 genes in initiation of zebrafish epiboly. *Proc. Natl. Acad. Sci. USA*. 105:198–203. http://dx.doi.org/10.1073/pnas.0707948105

Edmondson, D.G., T.C. Cheng, P. Cserjesi, T. Chakraborty, and E.N. Olson. 1992. Analysis of the myogenin promoter reveals an indirect pathway for positive autoregulation mediated by the muscle-specific enhancer factor MEF-2. *Mol. Cell. Biol.* 12:3665–3677.

Gerdes, J., H. Lemke, H. Baisch, H.H. Wacker, U. Schwab, and H. Stein. 1984. Cell cycle analysis of a cell proliferation-associated human nuclear antigen defined by the monoclonal antibody Ki-67. *J. Immunol.* 133:1710–1715.

Goecks, J., A. Nekrutenko, and J. Taylor; Galaxy Team. 2010. Galaxy: a comprehensive approach for supporting accessible, reproducible, and transparent computational research in the life sciences. *Genome Biol.* 11:R86. http://dx.doi.org/10.1186/gb-2010-11-8-r86

Gonzalez-Gutierrez, G., E. Miranda-Laferte, A. Neely, and P. Hidalgo. 2007. The Src homology 3 domain of the beta-subunit of voltage-gated calcium channels promotes endocytosis via dynamin interaction. *J. Biol. Chem.* 282:2156–2162. http://dx.doi.org/10.1074/jbc.M609071200

Gregg, R.G., A. Messing, C. Strube, M. Beurg, R. Moss, M. Behan, M. Sukhareva, S. Haynes, J.A. Powell, R. Coronado, and P.A. Powers. 1996. Absence of the beta subunit (cchb1) of the skeletal muscle dihydropyridine receptor alters expression of the alpha 1 subunit and eliminates excitation-contraction coupling. *Proc. Natl. Acad. Sci. USA*. 93:13961–13966. http://dx.doi.org/10.1073/pnas.93.24.13961

Griffin, C.A., L.H. Apponi, K.K. Long, and G.K. Pavlath. 2010. Chemokine expression and control of muscle cell migration during myogenesis. *J. Cell Sci.* 123:3052–3060. http://dx.doi.org/10.1242/jcs.066241

Grueter, C.E., S.A. Abiria, I. Dzhura, Y. Wu, A.J. Ham, P.J. Mohler, M.E. Anderson, and R.J. Colbran. 2006. L-type Ca2+ channel facilitation mediated by phosphorylation of the beta subunit by CaMKII. *Mol. Cell*. 23:641–650. http://dx.doi.org/10.1016/j.molcel.2006.07.006

Gupta, S., J.A. Stamatoyannopoulos, T.L. Bailey, and W.S. Noble. 2007. Quantifying similarity between motifs. *Genome Biol.* 8:R24. http://dx.doi.org/10.1186/gb-2007-8-2-r24

Hibino, H., R. Pironkova, O. Onwumere, M. Rousset, P. Charnet, A.J. Hudspeth, and F. Lesage. 2003. Direct interaction with a nuclear protein and regulation of gene silencing by a variant of the Ca2+-channel beta 4 subunit. *Proc. Natl. Acad. Sci. USA*. 100:307–312. http://dx.doi.org/10.1073/pnas.0136791100

Hicks, G.R., and N.V. Raikhel. 1995. Protein import into the nucleus: an integrated view. *Annu. Rev. Cell Dev. Biol.* 11:155–188. http://dx.doi.org/10.1146/annurev.cb.11.110195.001103

Hidalgo, P., and A. Neely. 2007. Multiplicity of protein interactions and functions of the voltage-gated calcium channel beta-subunit. *Cell Calcium*. 42:389–396. http://dx.doi.org/10.1016/j.ceca.2007.05.009

Hitt, M., A. Bett, L. Prevec, and F. Graham. 1998. Construction and propagation of human adenovirus vectors. *In* Cell Biology. J.E. Celis, editor. Academic Press. San Diego, CA. 1500–1512.

Hohaus, A., V. Person, J. Behlke, J. Schaper, I. Morano, and H. Haase. 2002. The carboxyl-terminal region of ahnak provides a link between cardiac L-type Ca2+ channels and the actin-based cytoskeleton. *FASEB J.* 16:1205–1216. http://dx.doi.org/10.1096/fj.01-0855com

Holden, N.S., and C.E. Tacon. 2011. Principles and problems of the electrophoretic mobility shift assay. *J. Pharmacol. Toxicol. Methods*. 63:7–14. http://dx.doi.org/10.1016/j.vascn.2010.03.002

Huang, W., B.T. Sherman, and R.A. Lempicki. 2009. Systematic and integrative analysis of large gene lists using DAVID bioinformatics resources. *Nat. Protoc.* 4:44–57. http://dx.doi.org/10.1038/nprot.2008.211

Kent, W.J., C.W. Sugnet, T.S. Furey, K.M. Roskin, T.H. Pringle, A.M. Zahler, and D. Haussler. 2002. The human genome browser at UCSC. *Genome Res.* 12:996–1006. http://dx.doi.org/10.1101/gr.229102

Kiyonaka, S., M. Wakamori, T. Miki, Y. Uriu, M. Nonaka, H. Bito, A.M. Beedle, E. Mori, Y. Hara, M. De Waard, et al. 2007. RIM1 confers sustained activity and neurotransmitter vesicle anchoring to presynaptic Ca2+ channels. *Nat. Neurosci.* 10:691–701. http://dx.doi.org/10.1038/nn1904

Knudson, C.M., N. Chaudhari, A.H. Sharp, J.A. Powell, K.G. Beam, and K.P. Campbell. 1989. Specific absence of the alpha 1 subunit of the dihydropyridine receptor in mice with muscular dysgenesis. *J. Biol. Chem.* 264:1345–1348.

Kuan, P.F., H. Chun, and S. Keleş. 2008. CMARRT: a tool for the analysis of ChIP-chip data from tiling arrays by incorporating the correlation structure. *Pac. Symp. Biocomput.* 2008:515–526.

Lacerda, A.E., H.S. Kim, P. Ruth, E. Perez-Reyes, V. Flockerzi, F. Hofmann, L. Birnbaumer, and A.M. Brown. 1991. Normalization of current kinetics by interaction between the alpha 1 and beta subunits of the skeletal muscle dihydropyridine-sensitive Ca2+ channel. *Nature*. 352:527–530. http://dx.doi.org/10.1038/352527a0

Laemmli, U.K. 1970. Cleavage of structural proteins during the assembly of the head of bacteriophage T4. *Nature*. 227:680–685. http://dx.doi.org/10.1038/227680a0

Le Grand, F., G. Auda-Boucher, D. Levitsky, T. Rouaud, J. Fontaine-Pérus, and M.F. Gardahaut. 2004. Endothelial cells within embryonic skeletal muscles: a potential source of myogenic progenitors. *Exp. Cell Res.* 301:232–241. http://dx.doi.org/10.1016/j.yexcr.2004.07.028

Leung, A.T., T. Imagawa, and K.P. Campbell. 1987. Structural characterization of the 1,4-dihydropyridine receptor of the voltage-dependent Ca2+ channel from rabbit skeletal muscle. Evidence for two distinct high molecular weight subunits. *J. Biol. Chem.* 262:7943–7946.

Leuranguer, V., S. Papadopoulos, and K.G. Beam. 2006. Organization of calcium channel beta1a subunits in triad junctions in skeletal muscle. *J. Biol. Chem.* 281:3521–3527. http://dx.doi.org/10.1074/jbc.M509566200

Leyris, J.P., C. Gondeau, A. Charnet, C. Delattre, M. Rousset, T. Cens, and P. Charnet. 2009. RGK GTPase-dependent CaV2.1 Ca2+ channel inhibition is independent of CaVbeta-subunit-induced current potentiation. *FASEB J.* 23:2627–2638. http://dx.doi.org/10.1096/fj.08-122135

Liu, Q.C., X.H. Zha, H. Faralli, H. Yin, C. Louis-Jeune, E. Perdiguero, E. Pranckeviciene, P. Muñoz-Cànoves, M.A. Rudnicki, M. Brand, et al. 2012. Comparative expression profiling identifies differential roles for Myogenin and p38α MAPK signaling in myogenesis. *J. Mol. Cell Biol.* 4:386–397. http://dx.doi.org/10.1093/jmcb/mjs045

Livak, K.J., and T.D. Schmittgen. 2001. Analysis of relative gene expression data using real-time quantitative PCR and the 2(-Delta Delta C(T)) Method. *Methods*. 25:402–408. http://dx.doi.org/10.1006/meth.2001.1262

Miranda-Laferte, E., G. Gonzalez-Gutierrez, S. Schmidt, A. Zeug, E.G. Ponimaskin, A. Neely, and P. Hidalgo. 2011. Homodimerization of the Src homology 3 domain of the calcium channel β-subunit drives dynamin-dependent endocytosis. *J. Biol. Chem.* 286:22203–22210. http://dx.doi.org/10.1074/jbc.M110.201871

Noyes, M.B., R.G. Christensen, A. Wakabayashi, G.D. Stormo, M.H. Brodsky, and S.A. Wolfe. 2008. Analysis of homeodomain specificities allows the family-wide prediction of preferred recognition sites. *Cell*. 133:1277–1289. http://dx.doi.org/10.1016/j.cell.2008.05.023

Ontell, M., M.P. Ontell, and M. Buckingham. 1995. Muscle-specific gene expression during myogenesis in the mouse. *Microsc. Res. Tech.* 30:354–365. http://dx.doi.org/10.1002/jemt.1070300503

Pai, A.C. 1965. Developmental genetics of a lethal mutation, muscular dysgenesis (Mdg), in the mouse. II. Developmental analysis. *Dev. Biol.* 11:93–109. http://dx.doi.org/10.1016/0012-1606(65)90039-4

Pinçon-Raymond, M., P. Vicart, P. Bois, O. Chassande, G. Romey, G. Varadi, Z.L. Li, M. Lazdunski, F. Rieger, and D. Paulin. 1991. Conditional immortalization of normal and dysgenic mouse muscle cells by the SV40 large T antigen under the vimentin promoter control. *Dev. Biol.* 148:517–528. http://dx.doi.org/10.1016/0012-1606(91)90270-D

Platzer, A.C. 1978. The ultrastructure of normal myogenesis in the limb of the mouse. *Anat. Rec.* 190:639–657. http://dx.doi.org/10.1002/ar.1091900303

Rando, T.A., and H.M. Blau. 1994. Primary mouse myoblast purification, characterization, and transplantation for cell-mediated gene therapy. *J. Cell Biol.* 125:1275–1287. http://dx.doi.org/10.1083/jcb.125.6.1275

Schredelseker, J., V. Di Biase, G.J. Obermair, E.T. Felder, B.E. Flucher, C. Franzini-Armstrong, and M. Grabner. 2005. The beta 1a subunit is essential for the assembly of dihydropyridine-receptor arrays in skeletal muscle. *Proc. Natl. Acad. Sci. USA*. 102:17219–17224. http://dx.doi.org/10.1073/pnas.0508710102

Schredelseker, J., A. Dayal, T. Schwerte, C. Franzini-Armstrong, and M. Grabner. 2009. Proper restoration of excitation-contraction coupling in the dihydropyridine receptor beta1-null zebrafish relaxed is an exclusive function of the beta1a subunit. *J. Biol. Chem.* 284:1242–1251. http://dx.doi.org/10.1074/jbc.M807767200

Schuster-Gossler, K., R. Cordes, and A. Gossler. 2007. Premature myogenic differentiation and depletion of progenitor cells cause severe muscle hypotrophy in Delta1 mutants. *Proc. Natl. Acad. Sci. USA*. 104:537–542. http://dx.doi.org/10.1073/pnas.0608281104

Smith, J., and D. Merrick. 2010. Embryonic skeletal muscle microexplant culture and isolation of skeletal muscle stem cells. *Methods Mol. Biol.* 633:29–56. http://dx.doi.org/10.1007/978-1-59745-019-5_3

Subramanyam, P., G.J. Obermair, S. Baumgartner, M. Gebhart, J. Striessnig, W.A. Kaufmann, S. Geley, and B.E. Flucher. 2009. Activity and calcium regulate nuclear targeting of the calcium channel beta4b subunit in nerve and muscle cells. *Channels (Austin)*. 3:343–355. http://dx.doi.org/10.4161/chan.3.5.9696

Tadmouri, A., S. Kiyonaka, M. Barbado, M. Rousset, K. Fablet, S. Sawamura, E. Bahembera, K. Pernet-Gallay, C. Arnoult, T. Miki, et al. 2012. Cacnb4 directly couples electrical activity to gene expression, a process defective in juvenile epilepsy. *EMBO J.* 31:3730–3744. http://dx.doi.org/10.1038/emboj.2012.226

Taher, L., N.M. Collette, D. Murugesh, E. Maxwell, I. Ovcharenko, and G.G. Loots. 2011. Global gene expression analysis of murine limb development. *PLoS ONE*. 6:e28358. http://dx.doi.org/10.1371/journal.pone.0028358

Takahashi, S.X., J. Miriyala, and H.M. Colecraft. 2004. Membrane-associated guanylate kinase-like properties of beta-subunits required for modulation of voltage-dependent Ca2+ channels. *Proc. Natl. Acad. Sci. USA*. 101:7193–7198. http://dx.doi.org/10.1073/pnas.0306665101

Takahashi, S.X., J. Miriyala, L.H. Tay, D.T. Yue, and H.M. Colecraft. 2005. A CaVbeta SH3/guanylate kinase domain interaction regulates multiple

properties of voltage-gated Ca2+ channels. *J. Gen. Physiol.* 126:365–377. http://dx.doi.org/10.1085/jgp.200509354

Takeshima, H., M. Iino, H. Takekura, M. Nishi, J. Kuno, O. Minowa, H. Takano, and T. Noda. 1994. Excitation-contraction uncoupling and muscular degeneration in mice lacking functional skeletal muscle ryanodine-receptor gene. *Nature*. 369:556–559. http://dx.doi.org/10.1038/369556a0

Taylor, J.R., Z. Zheng, Z.M. Wang, A.M. Payne, M.L. Messi, and O. Delbono. 2009. Increased CaVbeta1A expression with aging contributes to skeletal muscle weakness. *Aging Cell*. 8:584–594. http://dx.doi.org/10.1111/j.1474-9726.2009.00507.x

Tomczak, K.K., V.D. Marinescu, M.F. Ramoni, D. Sanoudou, F. Montanaro, M. Han, L.M. Kunkel, I.S. Kohane, and A.H. Beggs. 2004. Expression profiling and identification of novel genes involved in myogenic differentiation. *FASEB J.* 18:403–405.

Van Ho, A.T., S. Hayashi, D. Bröhl, F. Auradé, R. Rattenbach, and F. Relaix. 2011. Neural crest cell lineage restricts skeletal muscle progenitor cell differentiation through Neuregulin1-ErbB3 signaling. *Dev. Cell*. 21:273–287. http://dx.doi.org/10.1016/j.devcel.2011.06.019

Varadi, G., P. Lory, D. Schultz, M. Varadi, and A. Schwartz. 1991. Acceleration of activation and inactivation by the beta subunit of the skeletal muscle calcium channel. *Nature*. 352:159–162. http://dx.doi.org/10.1038/352159a0

Virolle, T., C. Coraux, O. Ferrigno, L. Cailleteau, J.P. Ortonne, P. Pognonec, and D. Aberdam. 2002. Binding of USF to a non-canonical E-box following stress results in a cell-specific derepression of the lama3 gene. *Nucleic Acids Res.* 30:1789–1798. http://dx.doi.org/10.1093/nar/30.8.1789

Washabaugh, C.H., M.P. Ontell, S.H. Shand, N. Bradbury, J.A. Kant, and M. Ontell. 2007. Neuronal control of myogenic regulatory factor accumulation in fetal muscle. *Dev. Dyn.* 236:732–745. http://dx.doi.org/10.1002/dvdy.21078

Yu, K., Q. Xiao, G. Cui, A. Lee, and H.C. Hartzell. 2008. The best disease-linked Cl- channel hBest1 regulates Ca V 1 (L-type) Ca2+ channels via src-homology-binding domains. *J. Neurosci.* 28:5660–5670. http://dx.doi.org/10.1523/JNEUROSCI.0065-08.2008

Zhang, Y., Y. Yamada, M. Fan, S.D. Bangaru, B. Lin, and J. Yang. 2010. The beta subunit of voltage-gated Ca2+ channels interacts with and regulates the activity of a novel isoform of Pax6. *J. Biol. Chem.* 285:2527–2536. http://dx.doi.org/10.1074/jbc.M109.022236

Zhou, W., L. Saint-Amant, H. Hirata, W.W. Cui, S.M. Sprague, and J.Y. Kuwada. 2006. Non-sense mutations in the dihydropyridine receptor beta1 gene, CACNB1, paralyze zebrafish relaxed mutants. *Cell Calcium*. 39:227–236. http://dx.doi.org/10.1016/j.ceca.2005.10.015

Zhu, L.J., C. Gazin, N.D. Lawson, H. Pagès, S.M. Lin, D.S. Lapointe, and M.R. Green. 2010. ChIPpeakAnno: a Bioconductor package to annotate ChIP-seq and ChIP-chip data. *BMC Bioinformatics*. 11:237. http://dx.doi.org/10.1186/1471-2105-11-237